ESTIMATING LOAD DISTRIBUTIONS FOR RETAINING STRUCTURES SUBJECTED TO RAILROAD LIVE LOADS

A Thesis

by

SEAN JOSEPH SMITH

Submitted to the Office of Graduate and Professional Studies of
Texas A&M University
in partial fulfillment of the requirements for the degree of

MASTER OF SCIENCE

Chair of Committee,	Gary Fry
Committee Members,	Charles Aubeny
	Alan Palazzolo
Head of Department,	Robin Autenrieth

August 2016

Major Subject: Civil Engineering

ABSTRACT

Retaining structures in proximity to railroads experience a variety of lateral loading intensities depending on the live load surcharge. Current design guidelines recommend using the Boussinesq solution for computing lateral loads due to stress influence of the surcharge load. Although this method provides a conservative approach for design of retaining structures, it employs various assumptions that are no longer valid in the cases of non-uniform soil conditions and structures with flexible responses to loading. As a result, a model that captures a closer estimate of soil-structure interaction behavior is desired.

An analytical model derived from beam theory is presented in this thesis. This model implements the method of initial parameters to solve for a beam equation for a 3rd-order distributed load. A program was written in Python to solve for the coefficients in the beam equation using a least squares regression. The inputs for this program are strain measurements to be obtained from a test site, and the outputs are the regression coefficients and stresses associated with the input strains. The motivation behind this approach is to analyze future experimental data for a retaining wall constructed at a test site in proximity to a railroad. Analysis of sample strain values produced a regression curve that closely matched the expected distributions associated with strain values. It was also found that the order of the regression could be adjusted if needed to reduce error of the resulting curves. Ultimately, the model produced in this research can be used for estimating loads on a full-scale test wall.

ACKNOWLEDGEMENTS

My thanks go to the chair of my committee, Dr. Gary Fry, and the members of my committee, Dr. Charles Aubeny and Dr. Alan Palazzolo, for their guidance with this research. They have provided the foundation of knowledge necessary to complete this project. I would also like to thank Union Pacific Railroad and Texas Department of Transportation for funding this research and constructing the test site. I am grateful for the support of the Center for Railway Research team, who contributed tremendously with the construction and instrumentation of the test site as well as the development of the diagrams and illustrations that gave me a better understanding of the previous work.

I would like to thank my family and friends for providing love and support throughout my graduate studies. Without their encouragement, I never would have mustered the strength to uproot my life for the sake of this investment in my future and am forever grateful to them for their patience.

Finally, I would like to express my sincerest gratitude for Mrs. Fan Disher, my former calculus teacher at Mandeville High School. Her dedication to students and diligent teaching style sparked a newfound interest in math and science that set me on a path toward successfully completing a graduate degree in engineering.

NOMENCLATURE

AASHTO	American Association of State Highway and Transportation Officials
a_i	Coefficient of distributed load polynomial
AISC	American Institute of Steel Construction
AREMA	American Railway Engineering and Maintenance-of-Way Association
ASD	Allowable Strength Design
ASTM	American Society for Testing and Materials
BNSF	Burlington Northern Santa Fe Railway
c	Distance from neutral axis to extreme fiber (in.)
C_i	Constant of integration
c_k	Coefficient of bending strain polynomial
d	Depth of cross-section (in.)
dA	Differential cross-sectional area (in.^{2})
DAQ	Data Acquisition
dF	Differential cross-sectional load (kips)
E	Elastic modulus (ksi)
f	Normal distribution density
F_G	Gage factor
FS	Factor of Safety

GTS	Guidelines for Temporary Shoring
I	Moment of inertia (in.^{4})
i	Index of sequence or sum
i_L	Current of left side of Wheatstone bridge (amperes)
i_R	Current of right side of Wheatstone bridge (amperes)
LRFD	Load and Resistance Factor Design
k	Row index of least squares summation
kHz	Kilohertz, 1000 units per second
kip	1000 pounds
ksi	Kips per square inch
l	Column index of least squares summation
L	Length of beam (in.)
lbs	Pounds
M	Bending moment (kip-in.)
m	Meters
M_0	Initial moment (kip-in.)
mm	Millimeters
n	Order of least squares regression polynomial
N	Sample size of statistical data
p_s	Lateral pressure (psf)
psf	Pounds per square foot
q	Surcharge pressure (psf)

R	Initial resistance (Ω)
R_a	Required strength using ASD load combinations
rad	Radians
R_i	Resistance of fixed resistor or strain gage (Ω)
R_n	Nominal strength
R_u	Required strength using LRFD load combinations
s	Standard deviation
S	Distance from shoring to centerline of track (ft)
t	Computation time (seconds)
T	Normalized computation time (unitless)
TxDOT	Texas Department of Transportation
UPRR	Union Pacific Railroad
V	Shear force (kips)
V_0	Initial shear (kips)
V_{AC}	Output voltage
V_{in}	Input voltage
w	Distributed load (kips/in.)
$\overline{w}$	Average load along differential segment (kips)
x	Distance along beam (in.)
y	Distance from neutral axis to cross-sectional fiber (in.)
z	Depth to point where pressure p_s is found (ft)
α	Angle between centerline of strip load to point z and wall (rad)

β	Angle between limits of strip load to point z (rad)
δ	Deflection of beam (in.)
δ_0	Initial deflection (in.)
ΔM	Change in bending moment (kip-in.)
ΔR	Change in resistance (Ω)
Δs	Change in cross-sectional segment length (in.)
ΔV	Change in shear (kips)
Δx	Differential segment length (in.)
$\Delta\Theta$	Curvature angle of differential segment (radians)
ε	Strain (in./in.)
ε_i	Strain of specified gage in Wheatstone bridge (in./in.)
ε_L	Longitudinal strain (in./in.)
ε_{max}	Extreme fiber strain (in./in.)
ε_T	Transverse strain (in./in.)
θ	Rotation angle (radians)
θ_0	Initial rotation (radians)
λ	Fractional location of average load along differential segment
μ	Statistical mean
ν	Poisson's ratio
ρ_0	Radius of curvature to neutral axis (in.)
σ	Normal stress (ksi)
σ_{max}	Extreme fiber stress (ksi)

σ_u	Ultimate stress (ksi)
σ_y	Yield stress (ksi)
ϕ	Strength reduction factor used in LRFD
Ω	Ohms, unit of electrical resistance

TABLE OF CONTENTS

Page

LIST OF FIGURES

Page

LIST OF TABLES

Page

1 INTRODUCTION

1.1 Introduction

Retaining walls and temporary shoring are used in railroad construction where excavations and re-grading are required. These structures consist of an exposed wall above the dredge line with backfill on the other side and in some cases a submerged portion below the excavation line for providing additional resistance. Various types of retaining structures are used for railroad use including gravity, pile, cantilever, anchored, and mechanically stabilized earth walls. Pile walls are the primary focus of this research. The two subtypes of pile walls that will be examined, soldier piles and sheet piles, are illustrated in Figure 1.

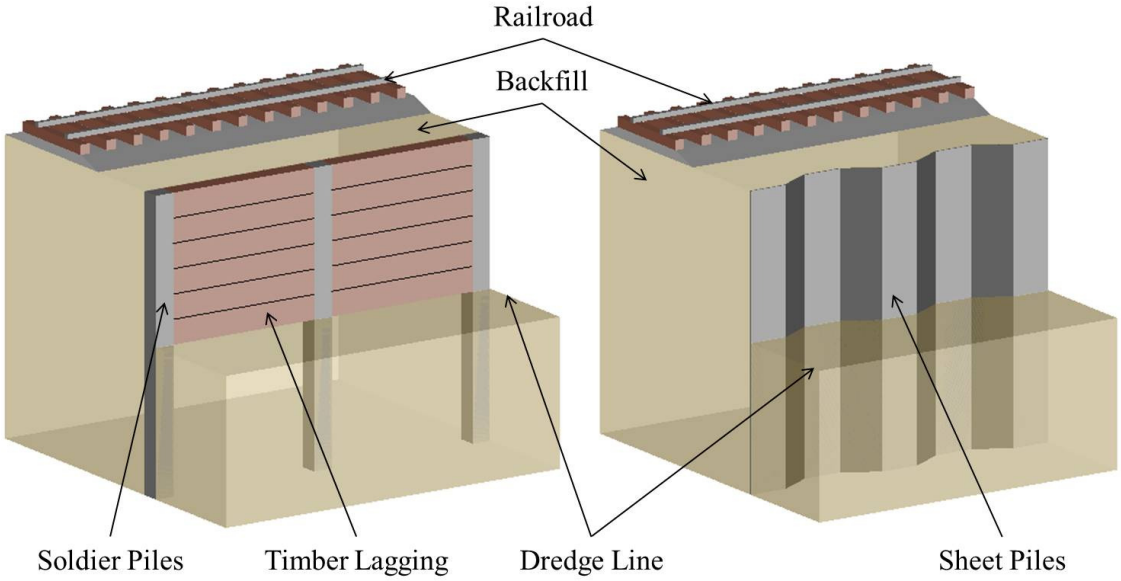

Figure 1 - Components of soldier and sheet pile walls

Railroads constructed on top of backfill produce loads that create a pressure distribution in the soil and retaining structure. Various methods are currently implemented to estimate these pressures for design purposes. However, the methods must impose assumptions about behavior of the soil and structure that may not be realistic in practice, such as keeping the structure rigid while calculating soil pressures. In reality, walls experience deflections and rotations that simultaneously affect the stresses in the wall and pressure distributions in the soil. This research will explore the effects of soil loading on retaining structures with the intent of providing a model that more closely couples load and effect in relation to the design of these structures.

1.2 Design Code Requirements

Current guidelines for design of retaining walls include the American Association of State Highway and Transportation Officials (AASHTO) Load and Resistance Factored Design (LRFD) Bridge Design Specifications (AASHTO, 2012) and the American Railway Engineering and Maintenance-of-Way Association Manual for Railway Engineering (AREMA, 2014). In addition, design of temporary shoring is described in the Guideline for Temporary Shoring (GTS) produced by Burlington Northern Santa Fe Railway (BNSF) and Union Pacific Railroad (UPRR) (2004). Although these guidelines provide some estimates of soil loads and retaining wall deflections, they do not fully address the behavior of walls under railroad live load surcharge. Retaining structures are flexible, and their response to soil loading must be considered as part of the design process in addition to the response of the soil mass itself.

The AREMA and GTS design codes calculate live load surcharge using Cooper E80 loading (AREMA, 2014; BNSF&UPRR, 2004). This method assumes a peak load of 80,000 lbs over a tie length of 9 ft and axle spacing of 5 ft. The associated surcharge pressure is calculated using Equation (1). This value is used to calculate lateral pressure acting on the structure using the Boussinesq solution, which applies elasticity theory to determine the influence of a surface load on earth pressure at a specified depth (Boussinesq, 1885).

$$q = \frac{80{,}000\ lbs}{(5\ ft)(9\ ft)} = 1778\ psf \quad \textbf{(1)}$$

The AASHTO, AREMA, and GTS design codes use the Boussinesq solution in (2) for calculating lateral earth pressure under a strip load and determining design loads on temporary shoring. The pressure distribution for this approach is shown in Figure 2. Although this method is based on elasticity theory, it makes various assumptions that only exist in ideal conditions. First, the solution assumes an infinitely large soil medium consisting of an ideal material with no variability in composition (Boussinesq, 1885). This assumption no longer holds true when discontinuities are present in the soil mass, such as in stratified soil or when an embedded structure providing resistance is present instead of an infinite medium. The apparent load experienced by the wall follows a different distribution as demonstrated by more recent experiments (Briaud et al., 1983; Smethurst & Powrie, 2007).

$$p_s = \frac{2q}{\pi}(\beta + \sin\beta \sin^2\alpha - \sin\beta\, cos^2\,\alpha) \quad \textbf{(2)}$$

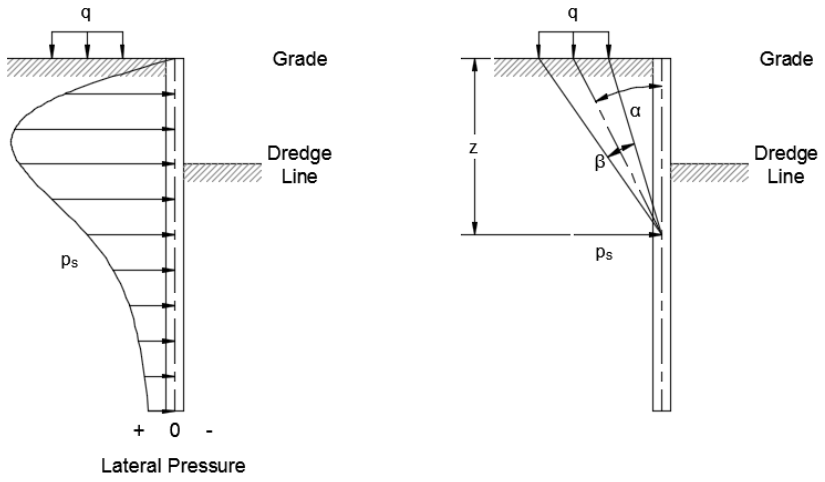

Figure 2 - Boussinesq solution for design lateral pressure (AASHTO, 2012; AREMA, 2014; BNSF&UPRR, 2004)

In addition to the disparity between theoretical and actual soil conditions, a retaining structure possesses flexibility parameters that are absent from the Boussinesq solution. The GTS code provides maximum deflection limits for temporary shoring. The limits are based on the perpendicular distance from the centerline of the track to the shoring. In addition, the vertical and horizontal deflection of the rail due to soil movement near the shoring system is provided by the GTS code. These values are listed in Table 1. The AREMA code specifies a maximum height of 12 ft for sheet pile and soldier pile walls in Chapter 8 Article 28.5.1.1 and Article 28.5.3.1. The associated relative tip deflections (δ/L) are 0.00260 for a maximum shoring deflection of 3/8 in. and 0.00347 for a deflection of 1/2 in. Previous research indicates that the deflection criteria in the GTS requirements exceed the limit for a rigid wall assumption, and these deflections may even occur after the soil has already mobilized (Sherif, 1984).

Table 1 - Deflection limits for temporary shoring systems (GTS, 2004)

Distance from shoring to centerline of track (ft)	Maximum horizontal deflection of shoring (in.)	Maximum horizontal or vertical deflection of rail (in.)
12 < S < 18	3/8	1/4
18 < S < 24	1/2	1/4

Various differences in design philosophies are considered in the construction of retaining structures. AREMA and GTS both use the Allowable Strength Design (ASD) philosophy for evaluating loads and limit states while AASHTO uses Load and Resistance Factor Design (LRFD). The American Institute of Steel Construction (AISC) Steel Construction Manual employs both methods for design. While ASD is commonly used in practice, it does not take advantage of a structure's full capacity nor does it account for the variability in service loads. Alternatively, LRFD provides load factors based on statistical data over many decades and strength reduction factors derived from many tests of a structural element's limit states. Equation (3) is the demand to capacity comparison for ASD while (4) is the comparison for LRFD.

$$R_a \leq \frac{R_n}{FS^1} \quad \textbf{(3)}$$

$$R_u \leq \phi R_n \quad \textbf{(4)}$$

One example of the differences between ASD and LRFD can be observed in AREMA Chapter 8 Article 28.5.3.4, which limits allowable stresses for cantilever

[1] AISC uses the Greek letter omega (Ω) instead of FS to indicate a factor of safety. However, Ω is used in this report as a unit of electrical resistance, Ohms.

soldier beam walls with lagging. The allowable stress for this structure is "2/3 tensile yield strength for steel" and further reduced stresses for recycled material (AREMA, 2014). Chapter 8 Article 28.6.3.2 then states that design stresses "shall not exceed those specified in the Manual of Steel Construction as published by AISC" (AREMA, 2014). However, AISC considers additional limit states, such as the full plastic capacity of flexural members, local buckling, and lateral torsional buckling, and applies strength reduction factors in addition to load factors for the demands (AISC, 2011). AASHTO also provides robust design requirements by separating specific loading conditions and defining specific load factors for each case (AASHTO, 2012). In addition, AASHTO implements strength reduction factors for various limit states using LRFD principles, similar to AISC.

1.3 Previous Research

Various experiments have been performed to more accurately predict the behavior of retaining structures under different loading conditions. The results from many of these studies conclude that the Boussinesq solution, which is commonly used in the design of retaining structures, tends to overestimate earth pressure loading and underestimate the flexibility of the structure. Some of these experiments utilize alternate methods of calculating lateral earth pressure, such as applying soil springs for developing P-y curves (Briaud, 1983). Despite the usability of these approximate methods, a closed-form solution for the observed lateral pressure on a retaining structure is not available.

Misra (1980) performed an analytical investigation of the Boussinesq solution and its effectiveness of estimating pressure distributions for various ratios of elastic to shear modulus. This approach was selected due to the variability of elastic properties for different types of backfill. In addition, changes in backfill type were introduced at varying depths to determine how an interface affects the pressure distribution. Ultimately, the researcher concluded that the existing model did not accurately determine the lateral pressure distribution for soft and loose soils that had poor shear stress transmission under a vertical load. The author also suggested that more experimentation on physical structures was required to produce more adequate estimates of stress distributions under realistic soil conditions.

A physical experiment was conducted by Briaud et al. (1983) to determine design pressures for retaining structures under railroad loads. The study instrumented two sheet pile walls with pressuremeters to estimate the stiffness of soil springs and used these values to develop deflection, shear, and moment curves under the finite difference method. This approach captures the flexibility of the wall by representing it as an Euler-Bernoulli beam and solving the fourth-order differential equation for deflection of a beam. The resulting pressure distribution is shown in Figure 3. When compared to the pressure distribution in Figure 2, it is apparent that the actual lateral pressure varies greatly from the theoretical pressure. As a result, the actual structural effects are not accurately estimated under the design pressures. One potential area of improvement with this study is to increase the number of pressuremeters behind the portion of the wall

above the dredge line. Only one pressuremeter was installed in this region, and the soil pressure distribution was approximated as a linear curve.

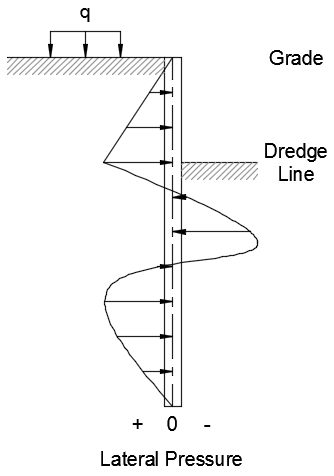

Figure 3 - Observed lateral pressure under strip load (Briaud et al., 1983)

Smethurst & Powrie (2007) investigated the effects of live loads on piles located on an embankment in proximity to a railroad. This experiment consisted of three auger-cast reinforced concrete piles instrumented with strain gages and inclinometers. The piles were 10 m in length and 0.6 m diameter with a spacing of 2.4 m. The instrumentation was embedded inside the concrete and attached to the reinforcement cage at various depths along the piles. Data was collected over a four year period, and average displacements, bending moments, and pressure distributions were calculated at various times. The results from this experiment found that pile displacements exceeded soil displacements over the majority of the pile length. In addition, the pressure distributions required to produce the associated bending moments varied from the

Boussinesq solution. A more accurate estimate of pressure and displacement was obtained using soil spring analysis, similar to the study conducted by Briaud (1983).

Sherif et al. (1982) performed an experiment to determine static and dynamic lateral earth pressures on a rigid retaining wall. A small scale test was constructed on a shake table and consisted of a 1 m tall movable aluminum plate on one side to simulate the wall and three boards with stiffeners for the remaining sides of the box. Load cells were placed between the wall and the actuators to obtain pressure data. In order to treat the wall as a rigid structure, the flexural stiffness was designed so that the maximum wall deflection was 0.05 mm. Over a height of 1 m, this corresponded to a relative displacement of 0.00005. This rigid wall assumption was later supported by similar research performed on the same test frame (Sherif et al., 1984). The purpose of this later experiment was to determine the coefficients of active earth pressure when the soil becomes mobilized. The results from this experiment showed that as wall deflection increased, lateral earth pressure dropped significantly, and the active stress was eventually achieved at a displacement of approximately 0.3 mm. This corresponds to a relative displacement of 0.0003.

A small scale test was conducted by Huang et al. (1999) to determine the influence of different wall rigidities on lateral pressure distribution. This experiment consisted of an aluminum plate representing a retaining wall and stacked steel rods oriented laterally and parallel to the plate representing a granular, cohesionless backfill. This approach was selected in order to easily observe the failure surfaces of the backfill. The backfill transferred lateral pressure to the plate using load cells, which were stacked

vertically and separated the backfill from the plate. The researchers found that a wall can be approximated as rigid if the wall tip deflection is below a certain amount, but the lateral pressure drops if the wall tip deflection is great enough. Based on this information, wall flexibility must be taken into account in the computation of design lateral pressures if the surcharge load is great enough to cause a large relative deflection.

Although these studies indicate that wall flexibility must be taken into consideration for computing design lateral pressures, they do not provide a closed-form solution that calculates lateral pressure for a flexible wall. As a result, more research is needed to produce a more accurate model for calculating design loads.

1.4 Objective

The goal of this research is to produce a statistical model for estimating the live load distribution on a retaining structure under railroad loading. This is to be accomplished by deriving an expression for wall behavior using beam theory and applying a statistical regression. The following steps must be performed in order to complete the objective of this project:

1. Apply beam theory to derive an expression for behavior of the retaining wall under soil loading,
2. Develop a statistical model for the load distribution based on acquired strain gage data,
3. Create a computer program for conducting statistical analysis, and
4. Devise a testing plan for future work on a full-scale test site.

2 EXPERIMENTAL PROCEDURES

2.1 Beam Model Derivation

The first step of the experiment is to derive an expression for behavior of the retaining wall using beam theory. The structure can be represented as a cantilever beam with the support located at the dredge line. In order to determine the behavior of the structure, a derivation from Euler-Bernoulli beam theory must be performed to produce an expression that relates external forces to measured strains (Hibbeler, 2008). The full derivation of this expression is laid out in Appendix A with key steps discussed in this section. First the differential equations for relating external loads to internal forces and deflections are obtained. These equations are based on force equilibrium of an infinitesimal segment of a beam as shown in Figure 4.

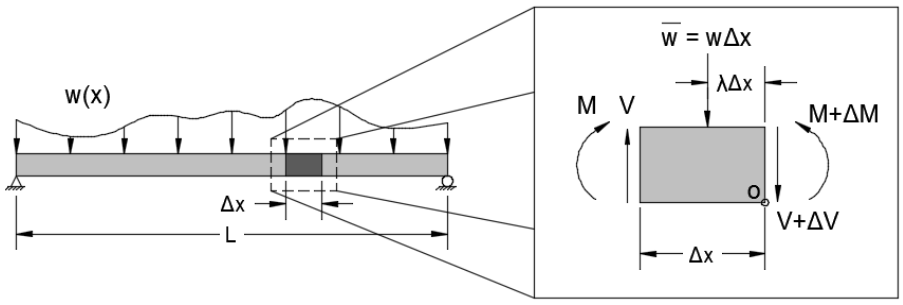

Figure 4 - General beam with free-body diagram of an infinitesimal segment

In addition to force equilibrium, a constitutive model must be applied to relate forces to deflections. This is accomplished by examining the internal stresses and resulting beam curvature under an applied moment as shown in Figure 5.

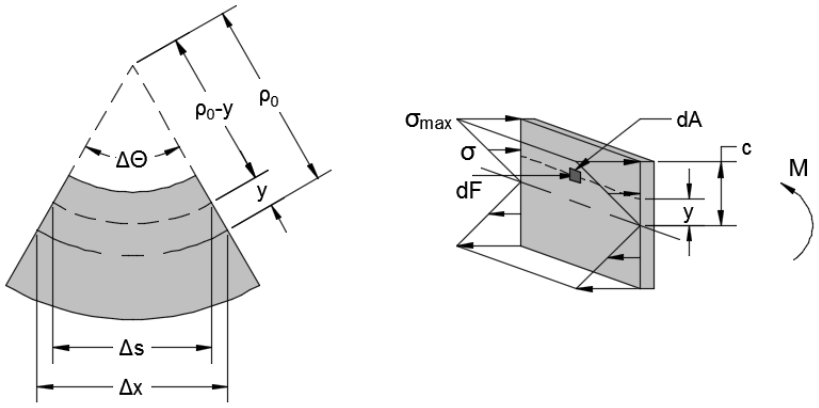

Figure 5 - Beam curvature and internal stress distribution under applied moment

The equilibrium conditions and constitutive relationship produce the set of differential equations indicated by (5) through (8).

$$\frac{dV}{dx} = -w(x) \tag{5}$$

$$\frac{dM}{dx} = V(x) \tag{6}$$

$$\frac{d\theta}{dx} = -\frac{M(x)}{EI} \tag{7}$$

$$\frac{d\delta}{dx} = \theta(x) \tag{8}$$

The method of initial parameters is one solution to these differential equations. Under this approach, the constants of integration are substituted with more convenient

terms that represent the values of deflection, slope, moment, and shear at the structure's reference point where $x = 0$ (Vlasov, 1966). The solutions under the method of initial parameters are shown in (9) through (12). In the case of the retaining wall, the dredge line is selected as the reference point. The free body diagram of the wall is shown in Figure 6 with positive sign convention indicated for the distributed load, slope, deflection, and initial parameters.

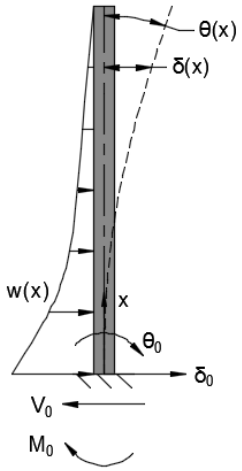

Figure 6 - Loading and deflection of retaining wall with initial parameters shown

$$V(x) = V_0 - \int_0^x w(s)ds \tag{9}$$

$$M(x) = M_0 + V_0 x - \int_0^x w(s)(x-s)ds \tag{10}$$

$$\theta(x) = \theta_0 - \frac{M_0 x}{EI} - \frac{V_0 x^2}{2EI} + \frac{1}{2EI}\int_0^x w(s)(x-s)^2 ds \tag{11}$$

$$\delta(x) = \delta_0 + \theta_0 x - \frac{M_0 x^2}{2EI} - \frac{V_0 x^3}{6EI} + \frac{1}{6EI}\int_0^x w(s)(x-s)^3 ds \tag{12}$$

The load distribution for the portion of the wall above the dredge line can be approximated as a third order polynomial as shown in (13). Coefficients a_0 through a_3 are unknown and determined through a regression analysis of the acquired data.

$$w(x) = a_0 + a_1 x + a_2 x^2 + a_3 x^3 \tag{13}$$

Substituting this expression into the integral portions of (9) through (12) and integrating produces the solutions shown in (14) through (17).

$$V(x) = V_0 - a_0 x - \frac{a_1 x^2}{2} - \frac{a_2 x^3}{3} - \frac{a_3 x^4}{4} \tag{14}$$

$$M(x) = M_0 + V_0 x - \frac{a_0 x^2}{2} - \frac{a_1 x^3}{6} - \frac{a_2 x^4}{12} - \frac{a_3 x^5}{20} \tag{15}$$

$$\theta(x) = \theta_0 - \frac{M_0 x}{EI} - \frac{V_0 x^2}{2EI} + \frac{a_0 x^3}{6EI} + \frac{a_1 x^4}{24EI} + \frac{a_2 x^5}{60EI} + \frac{a_3 x^6}{120EI} \tag{16}$$

$$\delta(x) = \delta_0 + \theta_0 x - \frac{M_0 x^2}{2EI} - \frac{V_0 x^3}{6EI} + \frac{a_0 x^4}{24EI} + \frac{a_1 x^5}{120EI} + \frac{a_2 x^6}{360EI} + \frac{a_3 x^7}{840EI} \tag{17}$$

2.2 Derivation of Regression Model

The expected results of the analysis are load distribution coefficients, initial shear and moment values, and the bending stress values for each data point. The acquired data is a set of strain values at each measurement time. In order to produce the expected results from the acquired data, an additional relationship between measured strain and the method of initial parameters solution must be defined. The derivation of this relationship is performed in Appendix A, and key steps are discussed below. First, bending strain and moment are related to each other through a linear-elastic constitutive model and force equilibrium of an infinitesimal segment of the beam as previously shown in Figure 5.

$$\varepsilon = \frac{\sigma}{E}$$

$$\sigma = \frac{My}{I}$$

$$\varepsilon = \frac{My}{EI} \tag{18}$$

The expression for bending moment in (15) is substituted into (18).

$$\varepsilon(x) = \frac{M_0 y}{EI} + \frac{V_0 yx}{EI} - \frac{a_0 yx^2}{2EI} - \frac{a_1 yx^3}{6EI} - \frac{a_2 yx^4}{12EI} - \frac{a_3 yx^5}{20EI} \tag{19}$$

The strain gages are located at a distance of $d/2$ from the neutral axes of the H-pile and sheet pile sections. Substituting this into (19) produces the expression shown in (20).

$$\varepsilon(x) = \frac{M_0 d}{2EI} + \frac{V_0 dx}{2EI} - \frac{a_0 dx^2}{4EI} - \frac{a_1 dx^3}{12EI} - \frac{a_2 dx^4}{24EI} - \frac{a_3 dx^5}{40EI} \tag{20}$$

This equation can be simplified into the fifth-order polynomial in (21).

$$\varepsilon(x) = c_0 + c_1 x + c_2 x^2 + c_3 x^3 + c_4 x^4 + c_5 x^5 \tag{21}$$

Where:

$$c_0 = \frac{M_0 d}{2EI} \qquad c_1 = \frac{V_0 d}{2EI} \qquad c_2 = -\frac{a_0 d}{4EI}$$

$$c_3 = -\frac{a_1 d}{12EI} \qquad c_4 = -\frac{a_2 d}{24EI} \qquad c_5 = -\frac{a_3 d}{40EI}$$

In order to solve for the coefficients based on acquired strain gage data, a least squares regression is implemented (Walpole et al., 2007). This method produces a polynomial of a specified order k for n input strain gages.

$$\left\{\sum_{i=0}^{n-1} \varepsilon_i x_i^k\right\} = \left[\sum_{i=0}^{n-1} x_i^{k+l}\right]\{c_k\} \tag{22}$$

Or in expanded form for a fifth order regression:

$$\begin{Bmatrix} \sum_{i=0}^{n-1} \varepsilon_i x_i^0 \\ \sum_{i=0}^{n-1} \varepsilon_i x_i^1 \\ \sum_{i=0}^{n-1} \varepsilon_i x_i^2 \\ \sum_{i=0}^{n-1} \varepsilon_i x_i^3 \\ \sum_{i=0}^{n-1} \varepsilon_i x_i^4 \\ \sum_{i=0}^{n-1} \varepsilon_i x_i^5 \end{Bmatrix} = \begin{bmatrix} \sum_{i=0}^{n-1} x_i^0 & \sum_{i=0}^{n-1} x_i^1 & \sum_{i=0}^{n-1} x_i^2 & \sum_{i=0}^{n-1} x_i^3 & \sum_{i=0}^{n-1} x_i^4 & \sum_{i=0}^{n-1} x_i^5 \\ \sum_{i=0}^{n-1} x_i^1 & \sum_{i=0}^{n-1} x_i^2 & \sum_{i=0}^{n-1} x_i^3 & \sum_{i=0}^{n-1} x_i^4 & \sum_{i=0}^{n-1} x_i^5 & \sum_{i=0}^{n-1} x_i^6 \\ \sum_{i=0}^{n-1} x_i^2 & \sum_{i=0}^{n-1} x_i^3 & \sum_{i=0}^{n-1} x_i^4 & \sum_{i=0}^{n-1} x_i^5 & \sum_{i=0}^{n-1} x_i^6 & \sum_{i=0}^{n-1} x_i^7 \\ \sum_{i=0}^{n-1} x_i^3 & \sum_{i=0}^{n-1} x_i^4 & \sum_{i=0}^{n-1} x_i^5 & \sum_{i=0}^{n-1} x_i^6 & \sum_{i=0}^{n-1} x_i^7 & \sum_{i=0}^{n-1} x_i^8 \\ \sum_{i=0}^{n-1} x_i^4 & \sum_{i=0}^{n-1} x_i^5 & \sum_{i=0}^{n-1} x_i^6 & \sum_{i=0}^{n-1} x_i^7 & \sum_{i=0}^{n-1} x_i^8 & \sum_{i=0}^{n-1} x_i^9 \\ \sum_{i=0}^{n-1} x_i^5 & \sum_{i=0}^{n-1} x_i^6 & \sum_{i=0}^{n-1} x_i^7 & \sum_{i=0}^{n-1} x_i^8 & \sum_{i=0}^{n-1} x_i^9 & \sum_{i=0}^{n-1} x_i^{10} \end{bmatrix} \begin{Bmatrix} c_0 \\ c_1 \\ c_2 \\ c_3 \\ c_4 \\ c_5 \end{Bmatrix}$$

After solving this system of equations, the initial parameters and load coefficients in (23) are calculated based on the obtained regression coefficients. These values are the desired result for further statistical analysis.

$$M_0 = \frac{2EIc_0}{d} \qquad V_0 = \frac{2EIc_1}{d} \qquad a_0 = -\frac{4EIc_2}{d}$$
$$a_1 = -\frac{12EIc_3}{d} \qquad a_2 = -\frac{24EIc_4}{d} \qquad a_3 = -\frac{40EIc_5}{d} \tag{23}$$

2.3 Development of Analysis Program

An analysis program, wall_stress.py, was written in Python. The purpose of this program was to implement the least squares regression described by (22) and produce the output parameters in (23). The program was written for Python version 3.5 and imported the native and external libraries listed in Table 2.

Table 2 - Python libraries implemented in wall_stress.py

Library	Native or External	Purpose
math	Native	Perform computations beyond arithmetical operations
numpy	External	Conduct matrix operations
openpyxl	External	Read and write data in Microsoft Excel
os	Native	Delete and create output files
time	Native	Measure performance of analysis program

Python was selected for this analysis due to its performance. For comparison, another program was developed in MATLAB that conducted identical operations including reading and writing of data. Using a set of debugging data, the MATLAB program completed the analysis in more time than the Python program. In addition, Python required less memory and computing power than MATLAB. Although Python exhibited greater performance, setup involved a significant amount of configuration, and each external library required manual installation and configuration. MATLAB required very little additional setup and did not require installation of external libraries. An in-depth comparison of performance between the two programs is conducted in Chapters 3 and 4.

2.4 Test Site Setup for Future Experimentation

In order to compare the analytical model to observed behavior of retaining structures, a full-scale test site was constructed in proximity to a railroad. This site consists of two types of retaining structures: a soldier pile wall and a sheet pile wall. The soldier pile wall consisted of three H-piles with timber lagging between the piles while the sheet pile wall consisted of individual repeating segments that were joined together. Each instrumented pile was given a station number from 1 to 5 as shown in Figure 7. Station 3 was the location where the soldier pile and sheet pile sections joined together and was subdivided into stations 3a and 3b, corresponding to the H-pile and sheet pile, respectively.

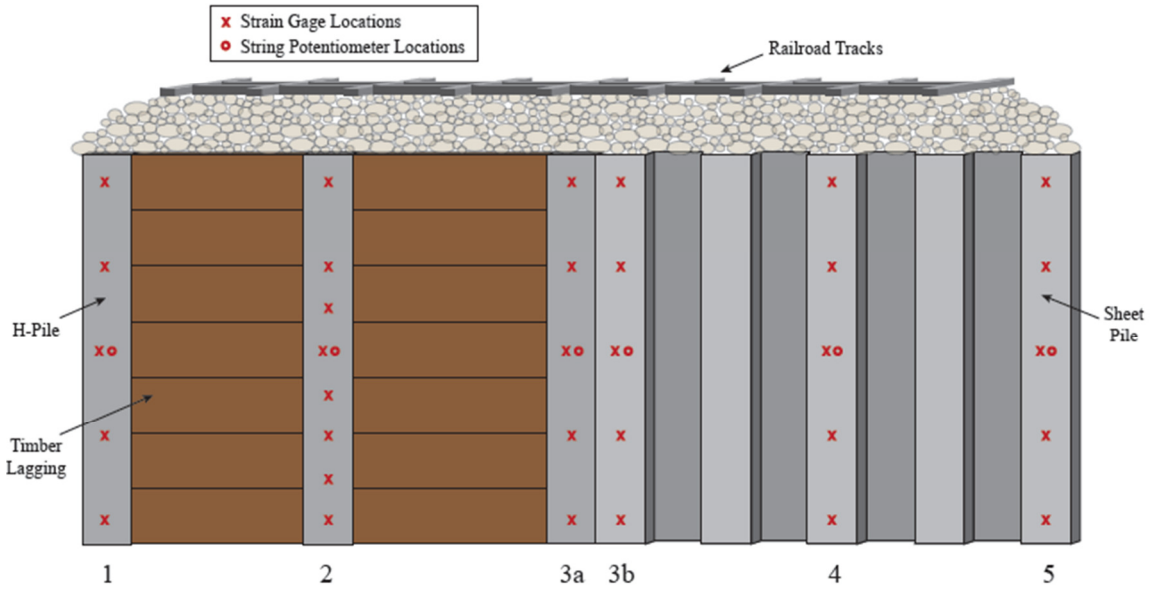

Figure 7 - Locations of instrumentation on test wall (Rachal, 2014)

The H-pile sections consist of HP12X84 shapes as shown in Figure 8. The most commonly used material for HP shapes is A572 Grade 50 structural steel with yield strength of 50 ksi and ultimate tensile strength of 65 ksi (AISC, 2011). The elastic modulus E for steel is 30,000 ksi (AREMA, 2014), and Poisson's ratio is 0.3 (AISC, 2011). This segment of the wall terminates with pile 3a where the sheet pile segment begins.

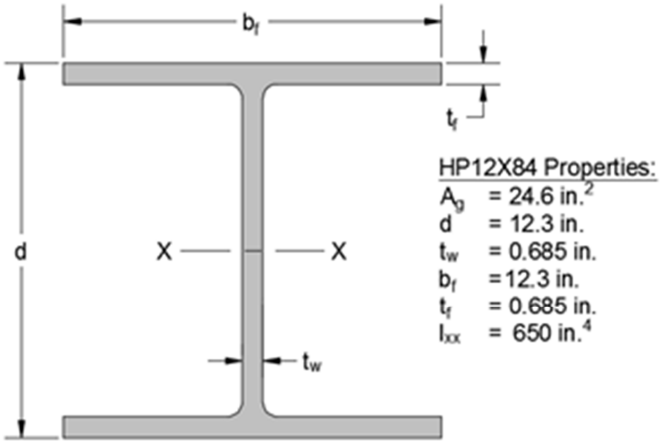

Figure 8 - HP12X84 section properties

The sheet pile sectional properties are to be determined as part of the future research discussed in Chapter 6. The two commonly used material specifications for these sections are A857 and A328 steel (ASTM, 2007; ASTM, 2013). A857 steel consists of three grades with different yield and tensile strengths. These values are listed in Table 3. A328 steel consists of a single grade with minimum yield strength of 39 ksi and minimum tensile strength of 65 ksi. As part of the future research plan, the specific

grade of steel for the sheet pile section of the wall must be determined in addition to the cross-sectional properties.

Table 3 - A857 steel grades and strengths (ASTM, 2007)

Grade	Yield Strength (ksi)	Tensile Strength (ksi)
30	30	49
33	33	52
36	36	53

In addition to determining the sectional and material properties, the dimensions of the wall and locations of the strain gages must be measured. These dimensions will be used for calculating the tributary areas of each soldier pile and the effective width of the sheet pile sections for their associated gage stations. In addition, the solution to the least squares regression described in (22) requires the locations of each strain gage.

2.5 Instrumentation Layout

Each H-pile is instrumented with strain gages and string potentiometers distributed along the compression face of the pile. Similarly, three compression faces of the sheet pile segment are also instrumented with strain gages and string potentiometers. Piles 1, 3a, 3b, 4, and 5 each have five longitudinal and five transverse strain gages distributed along the pile, and pile 2 has eight longitudinal and eight transverse strain gages. Each station is instrumented with one string potentiometer near midspan of the

pile. The strain gages are numbered with the first digit indicating the station number, second digit indicating the sequence along the pile starting with the letter V, and the third indicating whether the gage was oriented longitudinally (L) or transversely (T). For example, 3AXT represents the gage on station 3A, third gage up from the dredge line, and oriented transversely. The full layout and names of the strain gages are shown in Figure 9.

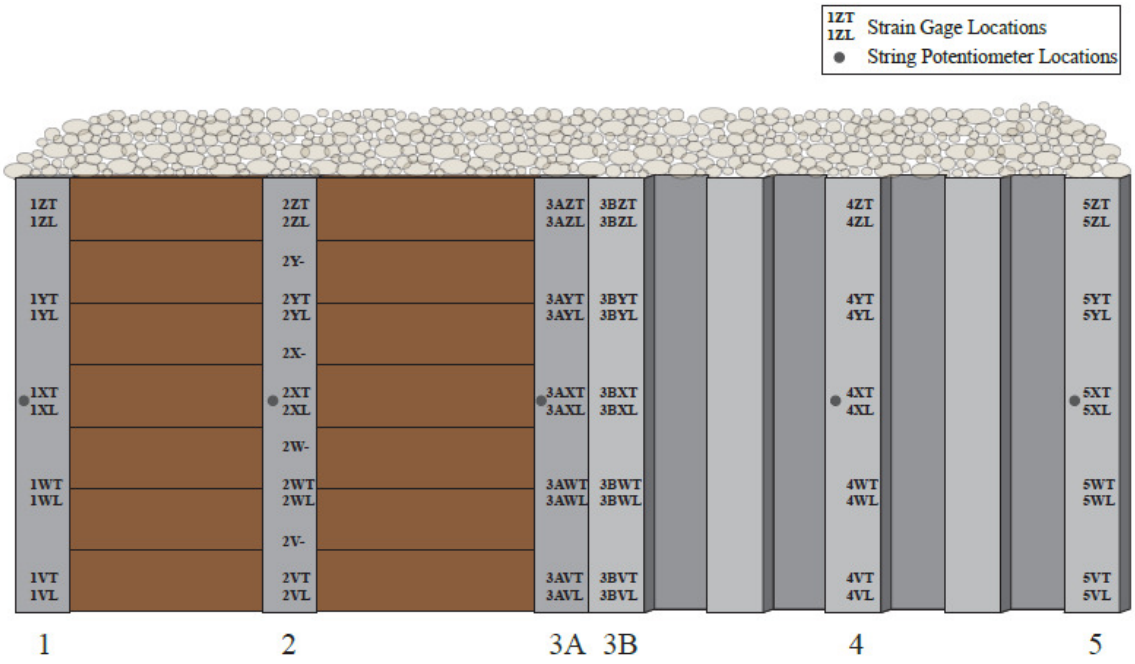

Figure 9 - Naming scheme for strain gages (Rachal, 2014)

2.6 Strain Gage Wiring

The strain gages are Tokyo Sokki Kenkyujo model AWC-8B-11-3LT weldable strain gages (Tokyo Sokki Kenkyujo, 2015). Each gage has base dimensions of 28x5

mm and a gage length of 8 mm. The base material is composed of stainless steel and has an operating temperature range of -20°C to +100°C with a self-correcting temperature compensation range of +10°C to +100°C. The rated resistance is 120±2 Ohms (Ω), and the gage factor is 2.04±2%. The gages were installed directly onto the piles using a spot welder.

Each strain gage is wired using a Wheatstone bridge configuration as shown in Figure 10. This circuit consists of an input voltage V_{in}, an output voltage V_{AC}, and four fixed resistors or variable resistance strain gages (Hoffmann, 1989). The circuit produces an output voltage when an imbalance forms between the currents i_L and i_R. If the resistors and strain gages are selected so that the initial output voltage is 0, then a change in voltage occurs when the resistance of any of the strain gages change. This change in resistance corresponds with mechanical and thermal strain in the base material as described by (24).

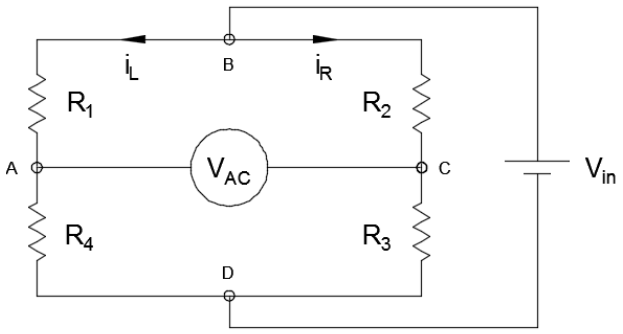

Figure 10 - Wheatstone bridge circuit diagram

$$F_G = \frac{\Delta R/R}{\Delta L/L} = \frac{\Delta R/R}{\varepsilon} \quad \textbf{(24)}$$

Common Wheatstone bridge configurations include full bridge, half bridge, and quarter bridge (Hoffmann, 1989). A summary of the number of fixed resistors and gages in each configuration is shown in Table 4. The general equation for output voltage of a Wheatstone bridge regardless of configuration is shown in (25).

Table 4 - Wheatstone bridge configuration summary

Configuration	Number of Fixed Resistors	Number of Strain Gages
Full Bridge	0	4
Half Bridge	2	2
Quarter Bridge	3	1

$$V_{AC} = V_{in}\left(\frac{R_4}{R_1 + R_4} - \frac{R_3}{R_2 + R_3}\right) \quad \textbf{(25)}$$

The strain gages can measure thermal or mechanical strain. In the case of the retaining wall, a half bridge configuration is used, which consists of a mechanical gage in the R_1 location, a thermal gage in the R_2 location, and two 120 Ω fixed resistors in the R_3 and R_4 locations. This resistance was selected to match that of the strain gages in an undeformed state. Output voltage was related to strain using (26), which is derived in Appendix B.

$$\varepsilon = \frac{1}{F_G}\left[\frac{1}{\frac{V_{AC}}{V_{in}} + \frac{1}{2}} - 2\right] \quad \textbf{(26)}$$

This expression applies to the longitudinally oriented strain gages. For the transversely oriented gages, this value is converted to longitudinal strain using Poisson's ratio as shown in (27).

$$\varepsilon_L = -\frac{\varepsilon_T}{\nu} \quad \textbf{(27)}$$

2.7 Data Acquisition System

The data acquisition (DAQ) system consists of a Strainbook/616 base module and Wavebook/516 expansion modules, all manufactured by IOtech. The strain gages are wired to the DAQ modules using custom soldered connections. The module stack is connected to a laptop containing Dasylab, the DAQ software. Input voltages, high and low pass filters, and bridge configurations for all channels are set in Dasylab. In addition, conversion of output voltages to strains and formatting of output files is defined in Dasylab as well. Data is collected at a rate of 1 kHz, or 1000 data points per second. The DAQ program is initiated by an excitation trigger that is activated when a train entered the test site to produce a voltage spike and terminated after the voltage has returned below a certain value for a specified amount of time.

3 ANALYSIS

3.1 Scope of Analysis

Because the suggested test plan defined in Chapter 6 was not yet implemented at the time of this project, the primary goals of analysis were to verify that the program accurately computed output parameters according to the theoretical model and to evaluate the performance of the analysis program. These goals were accomplished with the following steps:

1. Create sample input data,
2. Compute output parameters using analysis program,
3. Manually compute regression coefficients using Excel and compare with analysis program outputs,
4. Calculate and compare stresses from input strains and output regression curves, and
5. Write an equivalent analysis program in MATLAB and compare performance with Python program using statistical parameters.

3.2 Program Validation

The Python program was validated by manually calculating the regression curve for a sample data point and comparing the coefficients with those produced by the analysis program. Eight strain values were specified using (28) where ε_0 was selected as the yield strain. For grade 50 steel with an elastic modulus of 30,000 ksi, the associated

yield strain is 0.001667. The locations of the strain values began at a location of 0 ft and were spaced in 1 ft increments. The input strain values and locations are summarized in Table 5. The negative sign indicates compression because the experimental strain gages are installed on the compression face of the wall.

$$\varepsilon_i = \frac{\varepsilon_{i-1}}{2} \tag{28}$$

Table 5 - Input strain values and locations for program validation

Gage Location (ft)	Strain (in./in.)
0	-1.667×10^{-3}
1	-8.333×10^{-4}
2	-4.167×10^{-4}
3	-2.083×10^{-4}
4	-1.042×10^{-4}
5	-5.208×10^{-5}
6	-2.604×10^{-5}
7	-1.302×10^{-5}

These strain values were then analyzed using the program to produce the parameters in (23). After these values were obtained, the system of equations in (22) was solved in Excel to verify that the program output parameters matched those

calculated in Excel. The intent of this step was to ensure that no bugs were present in the program that would create a disparity between theoretical and experimental values.

3.3 Regression Analysis

After running the analysis on the input strain values listed in Table 5, the stresses directly associated with these strain values were compared with those computed using the output regression curve. For each input strain, the associated stress was calculated with (29).

$$\sigma = E\varepsilon \tag{29}$$

The stresses for the output regression were computed by taking (20) and substituting it into (29) to produce (30).

$$\sigma(x) = \frac{M_0 d}{2I} + \frac{V_0 dx}{2I} - \frac{a_0 dx^2}{4I} - \frac{a_1 dx^3}{12I} - \frac{a_2 dx^4}{24I} - \frac{a_3 dx^5}{40I} \tag{30}$$

These stresses were compared to each other by calculating the percent difference from directly computed stresses and regression stresses.

$$\%\, difference = \frac{|input\ \sigma - output\ \sigma|}{input\ \sigma} \times 100\% \tag{31}$$

3.4 Evaluation of Program Performance

A performance analysis was conducted to compare computation times between the Python program and a syntactically equivalent program written in MATLAB. Both programs were given the same input Excel file, which consisted of 60,000 data points for one strain gage station for one test. This simulated 60 seconds of data at a sample rate of

1 kHz. The analysis was conducted for both programs 50 times and analyzed using a normal distribution. The means were determined using (32) and sample standard deviations were calculated with (33).

$$\mu = \frac{1}{N}\sum_{i=1}^{N} t_i \tag{32}$$

$$s = \sqrt{\frac{1}{N-1}\sum_{i=1}^{N}(t_i - \mu)^2} \tag{33}$$

After these parameters were calculated, the normal distribution density was calculated using (34) (Walpole et al., 2007).

$$f(t) = \frac{1}{\sqrt{2\pi}s} e^{-\frac{1}{2}\left[\frac{t-\mu}{s}\right]^2} \tag{34}$$

4 RESULTS AND DISCUSSION

4.1 Test Load Distributions

Using the input strains in Table 5, the associated output parameters were computed through the analysis program. Simultaneously, the parameters were calculated in Excel for comparison. The results from both methods are listed in Table 6. In addition, the percent differences between the analysis methods for each parameter were calculated.

Table 6 - Comparison of program output parameters with Excel calculation

Parameter	Analysis Program	Excel	% Difference
M_0 (kip-in.)	-5284	-5284	0.004094
V_0 (kips)	299.7	298.9	0.2902
a_0 (kips/in.)	15.88	15.67	1.348
a_1 (kips/in.^{2})	-0.7099	-0.6846	3.694
a_2 (kips/in.^{3})	0.01137	0.01056	7.675
a_3 (kips/in.^{4})	-6.275x10^{-5}	-5.524x10^{-5}	13.594

An important observation of this comparison is that the percent difference increased as the order of magnitude of the output parameters decreased. This may be attributed to differences in precision between the two programs. For further comparison,

the output parameters were calculated using MATLAB, and the percent difference between these values and the Python program were computed as well. These results are shown in Table 7. In this case, the parameters were identical, which indicates that the two programs use the same precision for array computations.

Table 7 - Comparison of output parameters between Python and MATLAB

Parameter	Python	MATLAB	% Difference
M_0 (kip-in.)	-5284	-5284	0
V_0 (kips)	299.7	299.7	0
a_0 (kips/in.)	15.88	15.88	0
a_1 (kips/in.^{2})	-0.7099	-0.7099	0
a_2 (kips/in.^{3})	0.01137	0.01137	0
a_3 (kips/in.^{4})	-6.275x10^{-5}	-6.275x10^{-5}	0

The distributed load, shear, and moment curves for the computed output parameters were plotted for qualitative comparison. The parameters in Table 7 were substituted into (13) for distributed load, (14) for shear, and (15) for moment to produce the curves in Figure 11, Figure 12, and Figure 13, respectively.

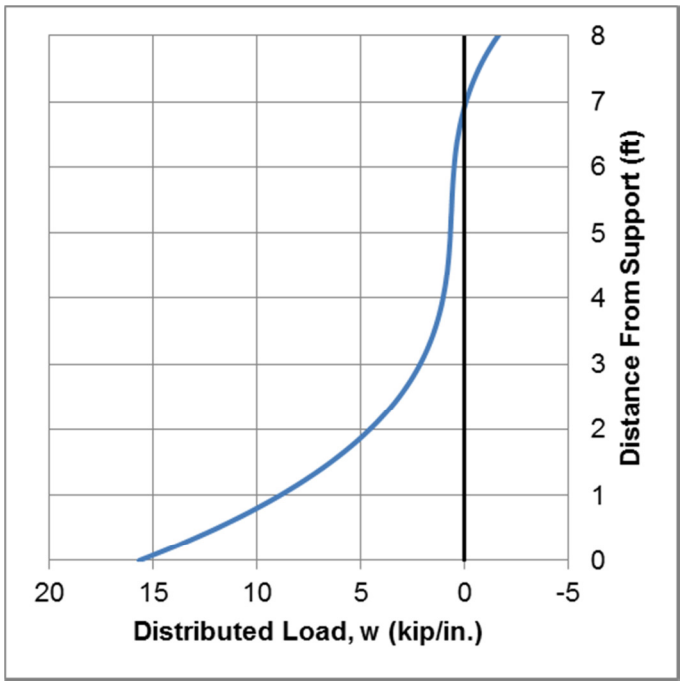

Figure 11 - Distributed load for program output parameters

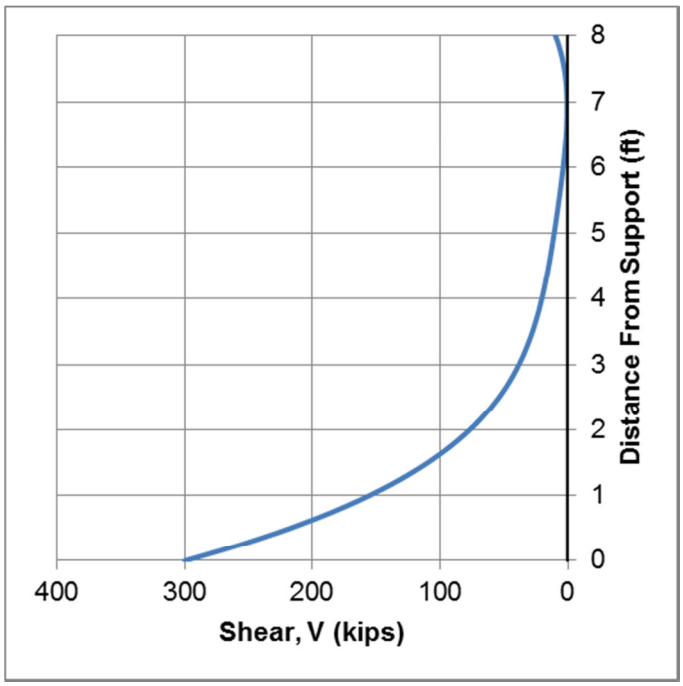

Figure 12 - Shear diagram for program output parameters

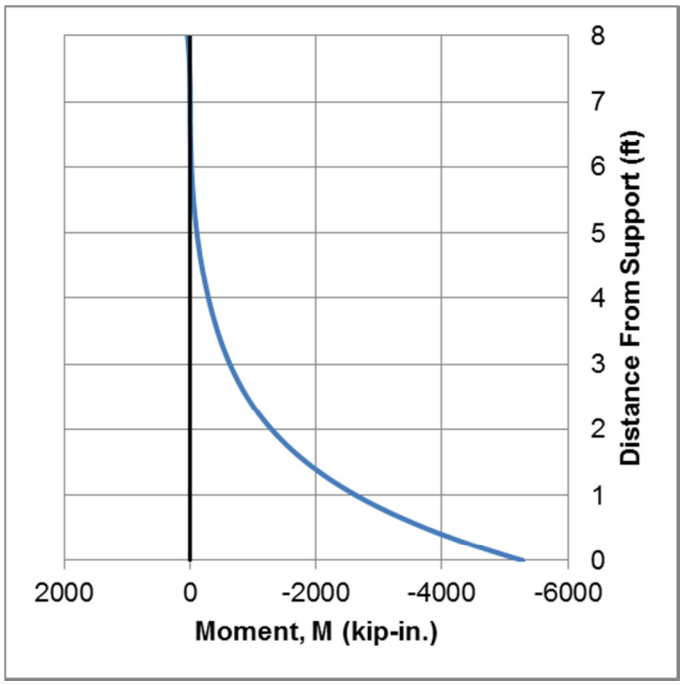

Figure 13 - Moment diagram for program output parameters

An important observation from these plots is that the distributed load becomes negative above 7 ft. This is indicative of passive pressure in the soil. Passive pressure has a stabilizing effect on the structure because it creates additional resistance against deflection. In reality, passive pressure may not be able to develop, and gapping could occur in this region which would result in an unloaded portion of the structure. If no load is present above a specific location, shear and moment would not be present either. As a result, any strain measurements above this point should have a value of 0 according to beam theory.

4.2 Comparison of Input and Output Stresses

After computing the regression coefficients, the associated stresses were calculated using the process described in Section 3.3. The stresses at each location were compared between direct computation from the measured strain and derived stress from the regression coefficients. The resulting values are listed in Table 8.

Table 8 - Comparison of measured and regression stresses

Location (ft)	Measured Stress (ksi)	Regression Stress (ksi)	Difference (ksi)	% Difference
0	-50.00	-50.00	0.004553	0.009105
1	-25.00	-24.94	0.06431	0.2572
2	-12.50	-12.25	0.2502	2.001
3	-6.250	-5.984	0.2663	4.260
4	-3.125	-2.765	0.3597	11.51
5	-1.563	-1.024	0.5381	34.44
6	-0.7813	-0.2122	0.5691	72.84
7	-0.3906	-0.02090	0.3697	94.65

In general, the stresses computed by the regression curve were smaller than those found directly from the measured strains. This difference was smaller for larger stresses near the support and increased with smaller stresses near the free end. A graphical comparison of the stresses is shown in Figure 14.

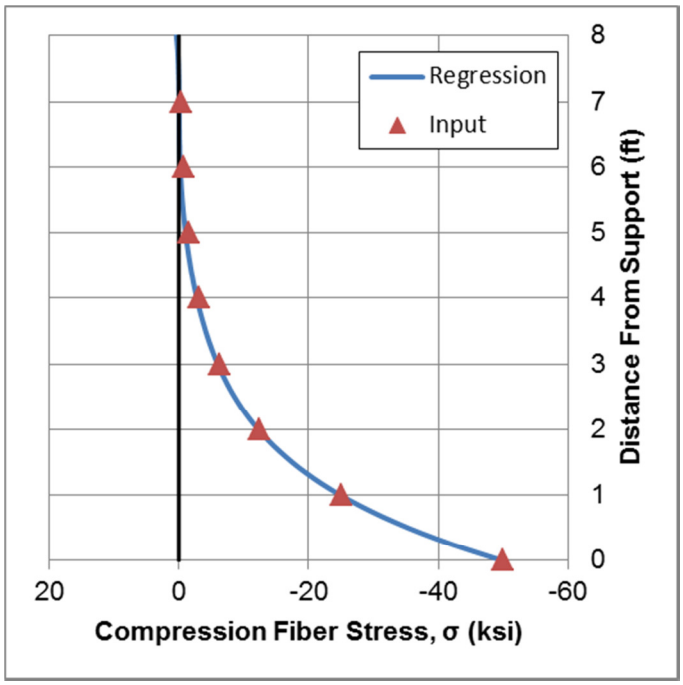

Figure 14 - Comparison of extreme compression fiber stresses

4.3 Comparison of Third and Fifth Order Load Distributions

In order to minimize the error between the measured and regression stresses, the order of the solution polynomial was increased to fifth order. This resulted in two additional terms in the load distribution that were carried through the beam theory derivation. The resulting load, shear, and moment equations are shown in (35) through (37).

$$w(x) = a_0 + a_1 x + a_2 x^2 + a_3 x^3 + a_4 x^4 + a_5 x^5 \quad \textbf{(35)}$$

$$V(x) = V_0 - a_0 x - \frac{a_1 x^2}{2} - \frac{a_2 x^3}{3} - \frac{a_3 x^4}{4} - \frac{a_4 x^5}{5} - \frac{a_5 x^6}{6} \quad \textbf{(36)}$$

$$M(x) = M_0 + V_0 x - \frac{a_0 x^2}{2} - \frac{a_1 x^3}{6} - \frac{a_2 x^4}{12} - \frac{a_3 x^5}{20} - \frac{a_4 x^6}{30} - \frac{a_5 x^7}{42} \quad \textbf{(37)}$$

Substituting the moment expression into (18) and (29) produced the strain and stress equations in (38) and (39).

$$\varepsilon(x) = \frac{M_0 d}{2EI} + \frac{V_0 dx}{2EI} - \frac{a_0 dx^2}{4EI} - \frac{a_1 dx^3}{12EI} - \frac{a_2 dx^4}{24EI} - \frac{a_3 dx^5}{40EI} - \frac{a_4 dx^6}{60EI} - \frac{a_5 dx^7}{84EI} \quad \textbf{(38)}$$

$$\sigma(x) = \frac{M_0 d}{2I} + \frac{V_0 dx}{2I} - \frac{a_0 dx^2}{4I} - \frac{a_1 dx^3}{12I} - \frac{a_2 dx^4}{24I} - \frac{a_3 dx^5}{40I} - \frac{a_4 dx^6}{60I} - \frac{a_5 dx^7}{84I} \quad \textbf{(39)}$$

After performing the regression analysis with these new expressions, the results in Table 9 were obtained. The magnitudes of the coefficients increased slightly for all parameters as a result of the additional terms.

Table 9 - Comparison of 3rd and 5th order polynomial load coefficients

Parameter	3rd Order Load	5th Order Load
M_0 (kip-in.)	-5284	-5285
V_0 (kips)	299.7	304.9
a_0 (kips/in.)	15.88	17.46
a_1 (kips/in.^{2})	-0.7099	-0.9720
a_2 (kips/in.^{3})	0.01137	0.02505
a_3 (kips/in.^{4})	-6.275×10^{-5}	-3.641×10^{-4}
a_4 (kips/in.^{5})	--	2.881×10^{-6}
a_5 (kips/in.^{6})	--	9.602×10^{-9}

The new distributed load, shear, and moment diagrams were plotted for the fifth order load distribution and are shown in Figure 15 through Figure 17. An immediate observation is that a region of negative load is present above 7 ft similar to the regression for the third order load distribution. However, the location that this sign change occurs is slightly further beyond 7 ft, and the magnitude is slightly less than the third order load.

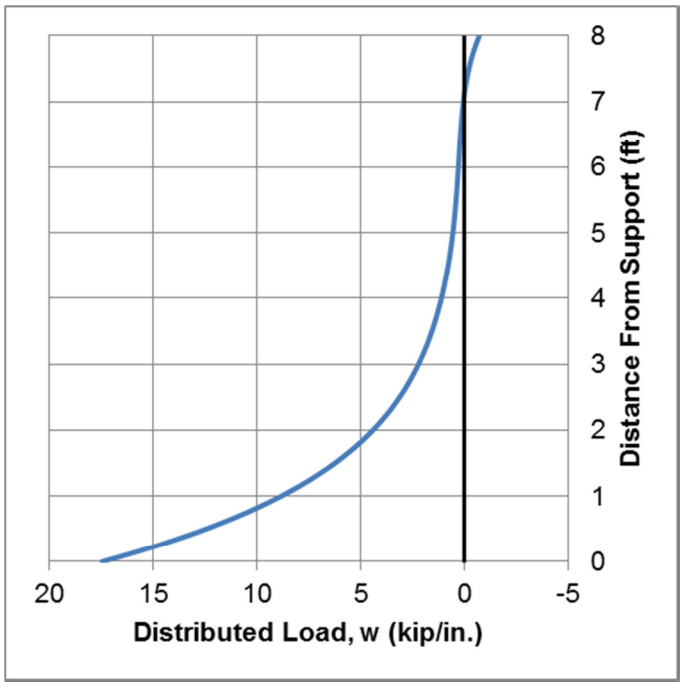

Figure 15 - Distributed load for 5th order load

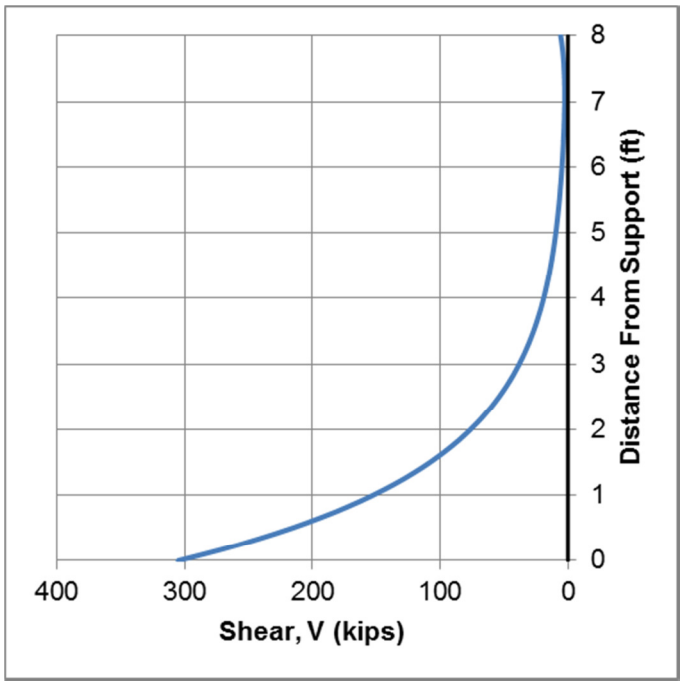

Figure 16 - Shear diagram for 5th order load

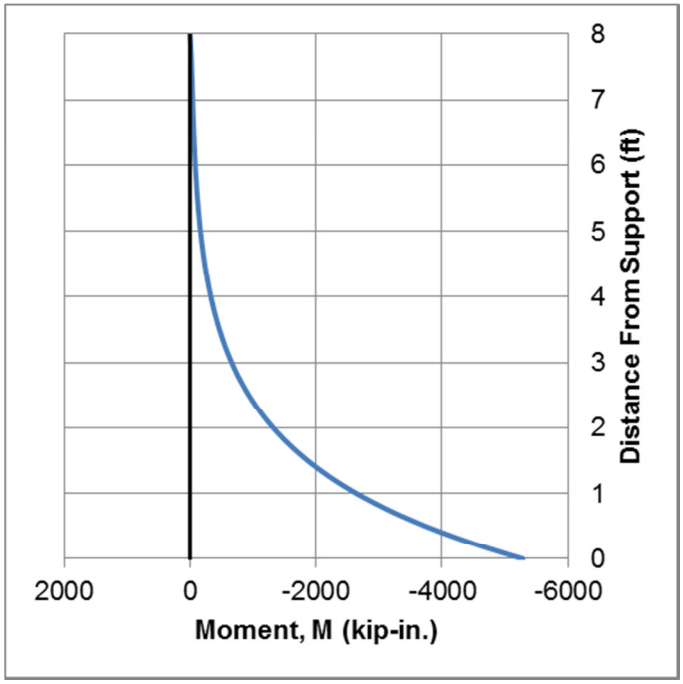

Figure 17 - Moment diagram for 5th order load

Next, the stresses were computed for the new regression curve and compared with those calculated from the sample strains. These results are listed in Table 10. Ultimately, the stresses computed from the regression curve were identical to those derived from the sample strains. This occurred because the number of output terms in the regression was equal to the number of measurements. This observation will be beneficial for future experimentation if the error in the output values is found to be unacceptable. The order of the regression polynomial can be adjusted until an optimum distribution is obtained that closely matches the directly measured data with minimal error.

Table 10 - Comparison of stresses for 5th order load distribution

Location (ft)	Measured Stress (ksi)	Regression Stress (ksi)	Difference (ksi)	% Difference
0	-50.00	-50.00	0	0
1	-25.00	-25.00	0	0
2	-12.50	-12.50	0	0
3	-6.250	-6.25	0	0
4	-3.125	-3.125	0	0
5	-1.563	-1.563	0	0
6	-0.7813	-0.7813	0	0
7	-0.3906	-0.3906	0	0

The associated stress distribution is plotted in Figure 18. Upon visual comparison of this plot with the stress distribution due to third order loading in Figure 14, it can be observed that the difference in stress between the two approaches is almost indecipherable. This indicates that the results from the third order polynomial have an acceptable level of error. However, the analysis program is capable of easily changing the output regression order if the error is found to be excessive.

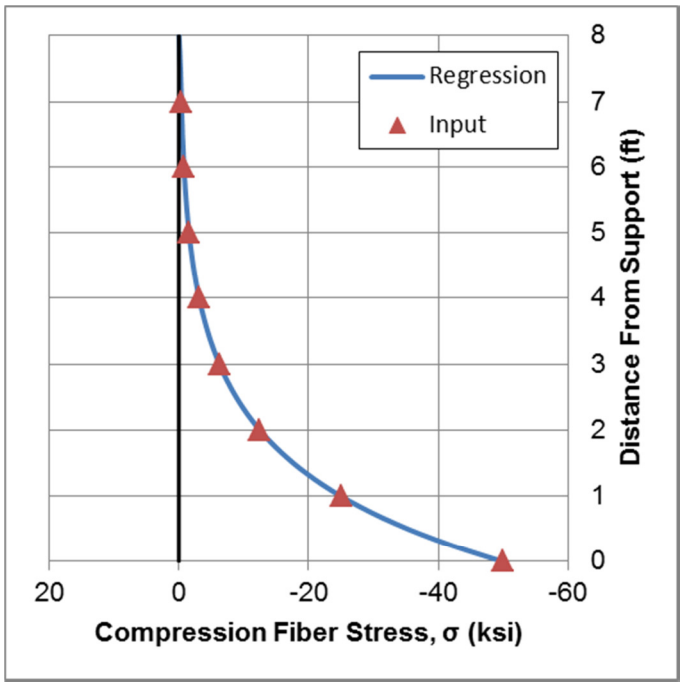

Figure 18 - Extreme compression fiber stress for 5th order load

4.4 Performance of Analysis Program

The performance of the Python program was analyzed using the methodology described in Section 3.4, which involved a sample size of 50 tests involving 60,000 data

points each. As part of this process, the performance of an equivalent MATLAB program was evaluated as well. The statistical parameters in Table 11 were calculated using (32) and (33). The mean computation time for Python was 43.557 seconds per station per test shorter than MATLAB. In addition, Python exhibited more precision than MATLAB with a standard deviation that was 0.708 seconds shorter.

Table 11 - Comparison of statistical parameters between Python and MATLAB analysis programs

Parameter	Python (seconds)	MATLAB (seconds)
Mean, μ	75.903	119.460
Standard Deviation, s	1.186	1.894
$\mu - 3s$	72.344	113.778
$\mu - 2s$	73.530	115.672
$\mu - 1s$	74.716	117.566
μ	75.903	119.460
$\mu + 1s$	77.089	121.354
$\mu + 2s$	78.275	123.248
$\mu + 3s$	79.461	125.142

The normal distributions for performance in both languages are shown in Figure 19. The difference between the maximum value for Python and minimum value for MATLAB was 33.019 seconds for the tested sample.

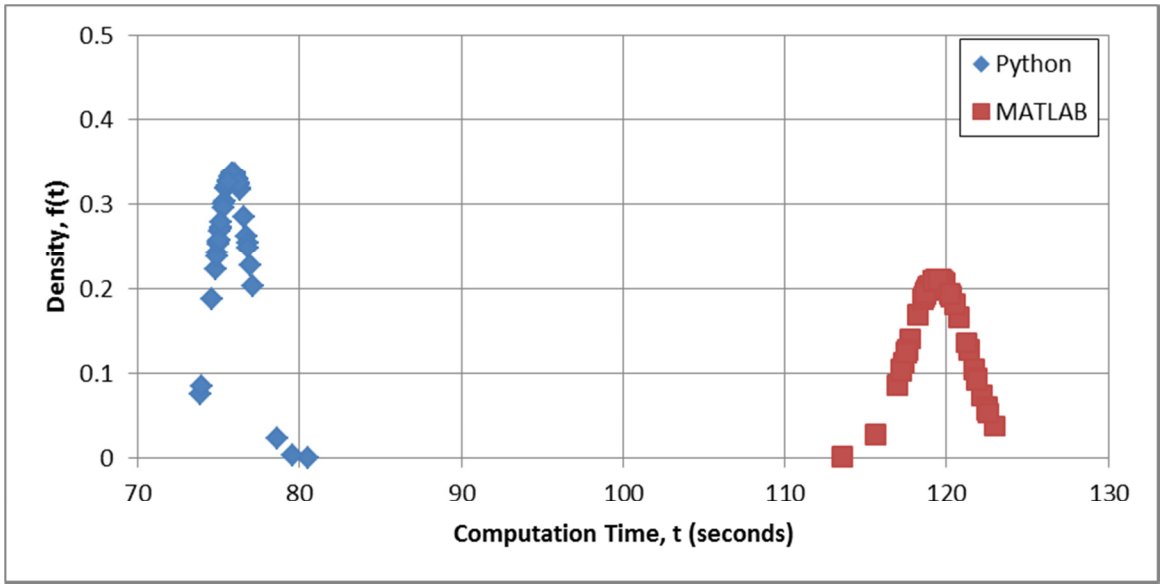

Figure 19 - Normal distributions of computation times

The distributions for both tests were examined separately in Figure 20 and Figure 21 to examine the difference between individual data points and the sample mean. More of Python's performance times were less than one standard deviation away from the mean than those of MATLAB. However, MATLAB exhibited fewer times above two standard deviations away from mean than Python.

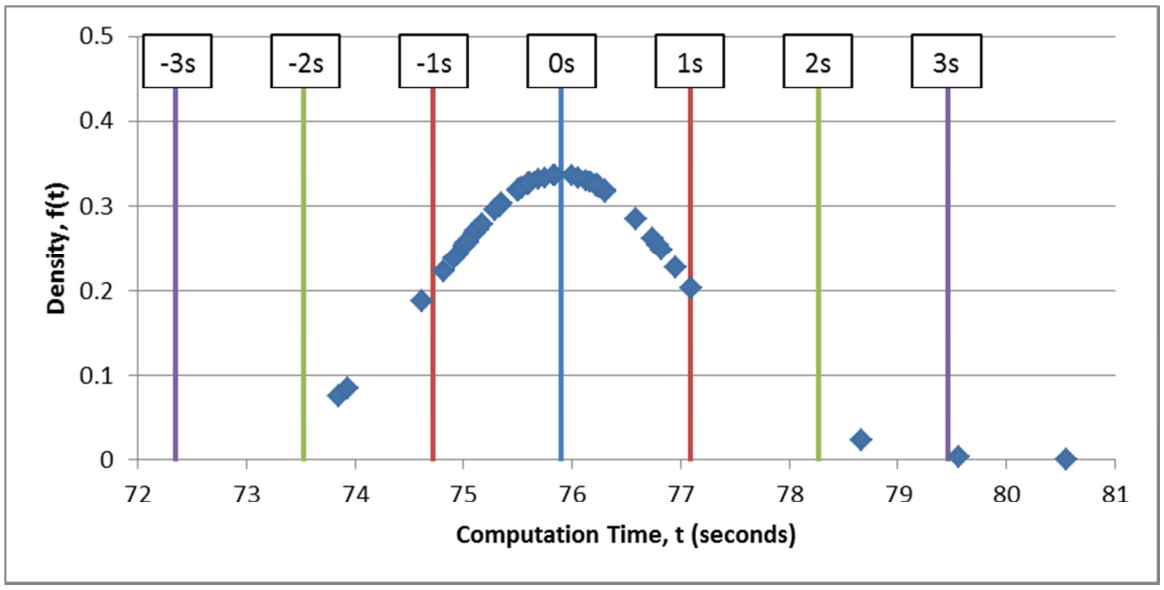

Figure 20 - Normal distribution of computation time for Python program

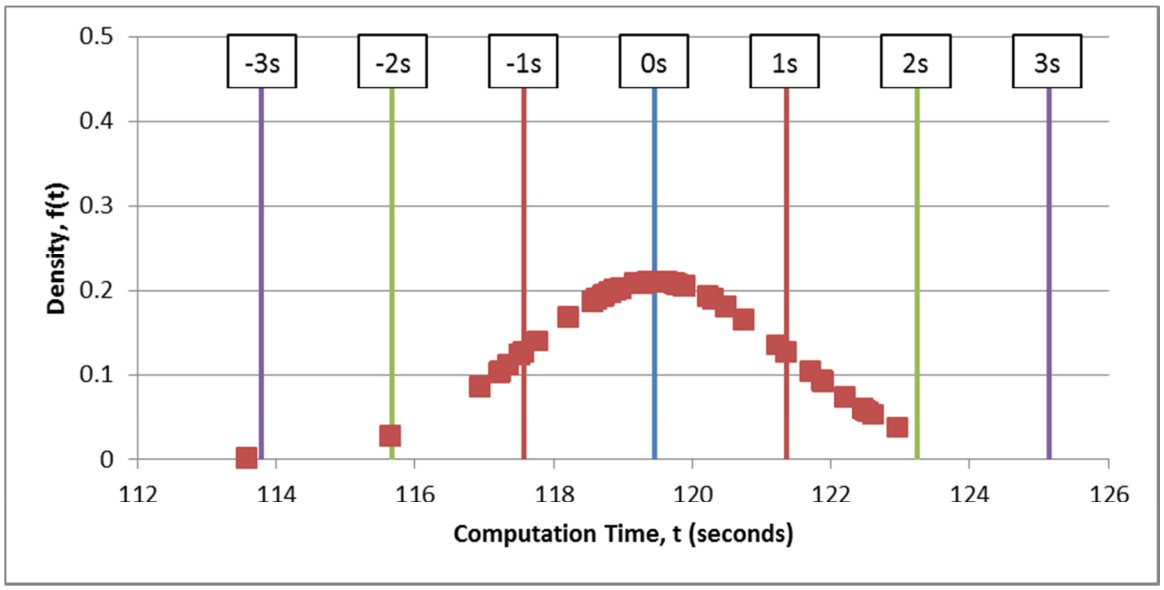

Figure 21 - Normal distribution of computation time for MATLAB program

The distributions were normalized to a mean of 0 seconds by subtracting the mean from each data point resulting in the distributions shown in Figure 22. The slope of the density function for the MATLAB results is flatter than the Python density function, which indicates that the computation time for Python is slightly more precise than MATLAB. This is supported by the larger standard deviation for MATLAB.

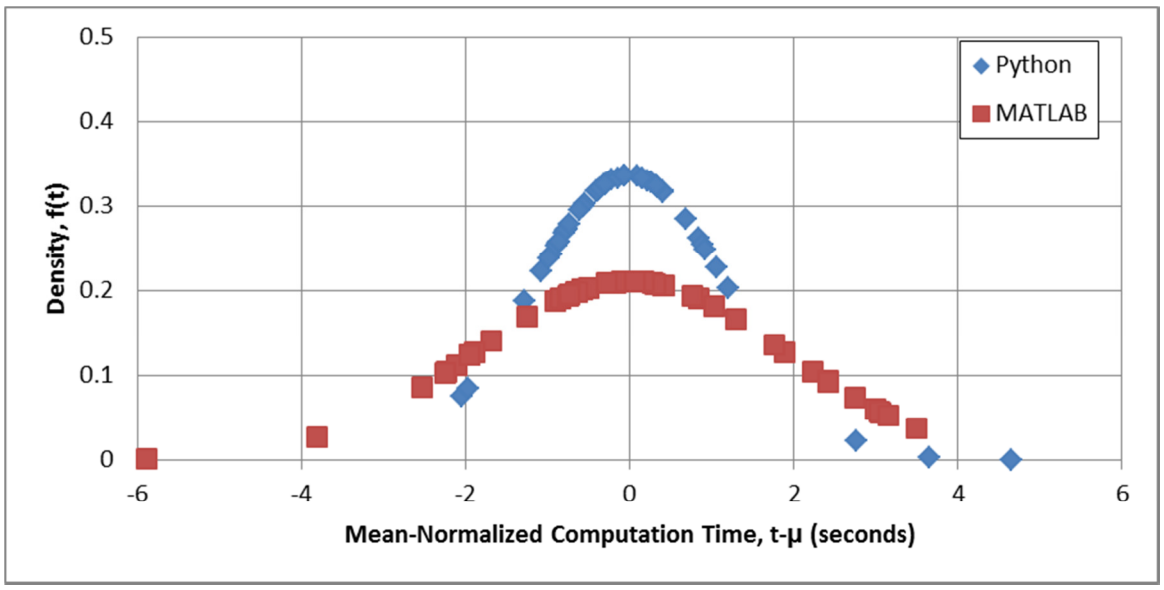

Figure 22 - Normal distributions of computation times adjusted to μ=0

5 CONCLUSIONS

The analytical model produced in this research provides a basis for estimating live loads on a full-scale test structure. By representing the structure as a beam, a system of equations was developed through beam theory and describes the relationship between load and effect. In addition, a procedure for relating these equations to acquired strain gage data was implemented in Python. The following results were the most significant observations from this research and provide a basis for future testing on the full-scale structure:

- The analytical model provides a strong approach for determining beam behavior under a third-order distributed load. This model can easily be adjusted for a polynomial of any order using the method of initial parameters.
- Regression coefficients computed with the analysis program were slightly different than those manually calculated using Excel. However, identical results were obtained between the Python and MATLAB versions of the program. This could be attributed to different methods of handling data types between the two languages and Excel.
- The stress values calculated from the output regression closely match those obtained directly from measured strains if the stresses are large but deviate if stresses are small. For a sample stress of 50 ksi, the associated percent difference was 0.009105%, but a sample stress of 0.3697 ksi had a percent difference of 94.65%.

- The error between the third order load distribution and the directly calculated stresses can be reduced or eliminated by increasing the order of the output polynomial. However, this adjustment may not be necessary with experimental data if the error is found to be at or below an acceptable level.
- The sample load distribution produced negative values above 7 ft. In an experimental test, this would indicate that either passive soil resistance is developing in this region or gapping has occurred. Ignoring passive resistance and assuming that gapping is present will result in a more conservative approach since passive resistance has a stabilizing effect on the structure.
- Better performance of the analysis program was observed when implemented in Python than in MATLAB. As a result, Python is recommended for analysis of actual measured strains.

6 FUTURE RESEARCH

Although this research provided a model for estimating live load effects of railroads on retaining walls under specific conditions, a full-scale test still needs to be performed. This test will require acquisition of data from multiple passing trains over the course of a few years to develop a statistically significant model of live loads. Although the test site is currently set up as described in Chapter 2, the following additional tasks need to be performed prior to future testing:

1. Install additional strain gages to the flanges of the HP sections in order to capture deformation of the cross-section.
2. Connect more data acquisition expansion modules for support of the additional gages.
3. Modify the landscape of the Dasylab acquisition program to account for new gages and expansion modules.
4. Verify all equipment is in working order and replace any damaged equipment, if present.
5. Acquire data for multiple trains and perform analysis using the program developed in this project.
6. Compare statistical loads from the acquired data with the Boussinesq solution used in design codes.
7. Prepare a report of preliminary findings to submit to the project stakeholders.

The testing methodology can be adjusted in the following ways to provide an estimate of loads under broader conditions:

1. Instrument wall with additional string potentiometers or inclinometers to determine changes in absolute deflections over time.
2. Instrument a wall with strain gages along the portion of the pile below the dredge line to determine full behavior of the piles.
3. Expand to test sites that involve skewed orientation of railroads relative to the retaining structure to determine the effects of lateral railroad loads on lateral earth pressure.
4. Investigate nonlinear behavior of the retaining structures, such as shear deformation, local buckling of sheet piles, and large deflections.

REFERENCES

American Association of State Highway and Transportation Officials (AASHTO) (2012). *AASHTO LRFD Bridge Design Specifications*. Washington, DC: AASHTO.

American Institute of Steel Construction (AISC) (2011). *AISC Steel Construction Manual*. Chicago, IL: AISC.

American Railway Engineering and Maintenance-of-Way Association (AREMA) (2014). *Manual for Railway Engineering.* Lanham, MD: AREMA.

American Society for Testing and Materials (ASTM) (2007). Standard Specification for Steel Sheet Piling, Cold Formed, Light Gage (ASTM Publication No. A857-07). West Conshohocken, PA: ASTM International.

American Society for Testing and Materials (ASTM) (2013). Standard Specification for Steel Sheet Piling (ASTM Publication No. A328-13a). West Conshohocken, PA: ASTM International.

Boussinesq, J. (1885). *Application des potentiels a l'étude de l'équilibre et du movement des solid élastiques*. Paris, France: Gauthier-Villars.

Briaud, J.L., Meriwether, M., Porwoll, H. (1983). *Pressuremeter Design of Retaining Walls* (FHWA/TX-83/340-4F). College Station, TX: Texas A&M Transportation Institute.

Burlington Northern Santa Fe Railway (BNSF), & Union Pacific Railroad (UPRR) (2004). Guidelines for Temporary Shoring. Kansas City, KS: BNSF; Omaha, NE: UPRR.

Hibbeler, R.C. (2008). *Mechanics of Materials* (7th ed.).Upper Saddle River, NJ: Pearson Prentice Hall.

Hoffmann, K. (1989). *An Introduction to Measurements using Strain Gages*. Darmstadt, Germany: Hottinger Baldwin Messtechnik GmbH.

Huang, C.C., Menq, F.Y., Chou, Y.C. (1999). The effect of the bending rigidity of a wall on lateral pressure distribution. *Canadian Geotechnical Journal*, 36 (6), 1039-1055.

Misra, B. (1980). Lateral pressures on retaining walls due to loads on surface of granular backfill. *Soils and Foundations,* 20 (2), 31-44.

Rachal, L (2014). Retaining wall instrumentation diagrams. College Station, TX: Texas A&M Transportation Institute, Center for Railway Research.

Sherif, M.A., Ishibashi, I., Lee, C.D. (1982). Earth pressures against rigid retaining walls. *Journal of the Geotechnical Engineering Division*, 108 (GT5), 679-695.

Sherif, M.A., Fang, Y.S., Sherif, R.I. (1984). K_A and K_0 behind rotating and non-yielding walls. *Journal of Geotechnical Engineering*, 110 (1), 41-56.

Smethurst, J.A., Powrie, W. (2007). Monitoring and analysis of the bending behavior of discrete piles used to stabilise a railway embankment. *Géotechnique*, 57 (8), 663-667.

Tokyo Sokki Kenkyujo Co. (2015). *Strain Gauges* (TML Pam E-1007A). Retrieved May 24, 2016 from: http://www.tml.jp/e/product/strain_gauge/catalog_pdf/AWseries.pdf

Vlasov, V.Z. (1966). *Beams, plates and shells on elastic foundations* (N. Leont′ev Trans.). Jerusalem, Israel: Israel Program for Scientific Translations.

Walpole, R.E., Myers, R.H., Myers, S.L., Ye, K. (2007). *Probability & Statistics for Engineers & Scientists* (8th ed.). Upper Saddle River, NJ: Pearson Prentice Hall.

APPENDIX A

DERIVATION OF BEAM EQUATIONS

The relationship between external load distribution and strain is derived using concepts from Euler-Bernoulli beam theory. The following equations provide a detailed approach to this derivation. The first step is to examine a general beam with a distributed load. An infinitesimal element is removed from the beam, and a free-body diagram is constructed displaying all internal and external forces.

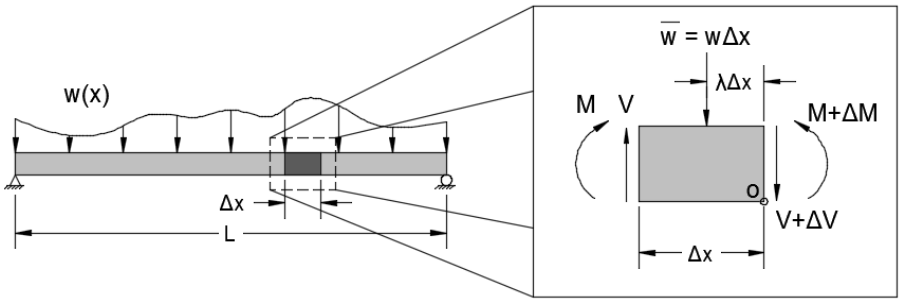

Equilibrium of the infinitesimal element is established for transverse forces and moments. Differential equations are obtained that relate change in shear to the distributed load and change in moment to shear.

$$\sum F_y = 0$$

$$V - w\Delta x - (V + \Delta V) = 0$$

$$\frac{\Delta V}{\Delta x} = -w$$

$$\lim_{\Delta x \to 0} \frac{\Delta V}{\Delta x} = \lim_{\Delta x \to 0} -w$$

$$\frac{dV}{dx} = -w(x)$$

$$\sum M\Big|_O = 0$$

$$(M + \Delta M) + w\lambda\Delta x^2 - M - V\Delta x = 0$$

$$\frac{\Delta M}{\Delta x} = V - w\lambda\Delta x$$

$$\lim_{\Delta x \to 0} \frac{\Delta M}{\Delta x} = \lim_{\Delta x \to 0} (V - w\lambda\Delta x)$$

$$\frac{dM}{dx} = V(x)$$

Because axial effects are negligible, an expression for force equilibrium in the axial direction is not necessary. The beam loads must then be related to slopes and deflections. This is accomplished by examining the stress and strain states of the loaded beam.

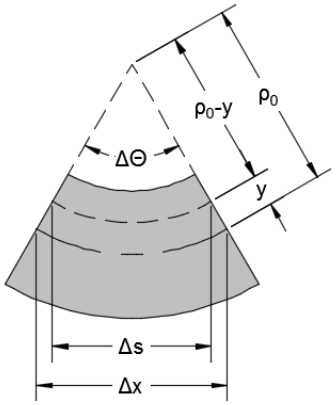

$$\varepsilon = \frac{\Delta s - \Delta x}{\Delta x}$$

$$\Delta s = (\rho_0 - y)\Delta\Theta$$

$$\Delta x = \rho_0\Delta\Theta$$

$$\varepsilon = \frac{(\rho_0 - y)\Delta\Theta - \rho_0\Delta\Theta}{\rho_0\Delta\Theta}$$

$$\varepsilon = -\frac{y}{\rho_0}$$

$$\frac{\varepsilon}{y} = -\frac{1}{\rho_0}$$

$$\varepsilon_{max} = -\frac{c}{\rho_0}$$

$$\frac{\varepsilon}{\varepsilon_{max}} = \frac{y}{c}$$

A linear-elastic constitutive model is applied to relate strain to stress.

$$\sigma = E\varepsilon$$

$$\frac{\sigma}{\sigma_{max}} = \frac{E\varepsilon}{E\varepsilon_{max}} = \frac{y}{c}$$

$$\sigma = \sigma_{max}\frac{y}{c}$$

$$\sigma_{max} = \sigma\frac{c}{y}$$

Moment equilibrium of an infinitesimal segment is taken to relate moment to flexural stress.

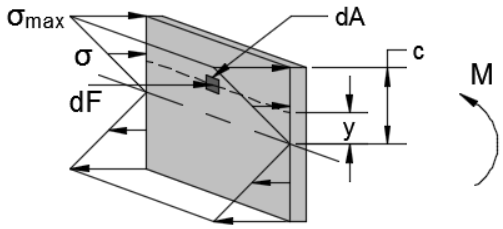

$$\sum M\Big|_{NA} = 0$$

$$M = \int_A ydF = \int_A y\sigma dA = \int_A y\sigma_{max}\frac{y}{c}dA$$

$$M = \frac{\sigma_{max}}{c}\int_A y^2 dA$$

$$M = \frac{\sigma_{max} I}{c}$$

$$M = \frac{\sigma I}{y}$$

$$\sigma = \frac{My}{I}$$

Flexural stress is substituted into the constitutive relationship to determine strain as a function of bending moment.

$$\varepsilon = \frac{\sigma}{E}$$

$$\varepsilon = \frac{My}{EI}$$

This equation is substituted into the strain-curvature relationship to develop the moment-curvature relationship.

$$\frac{M}{EI} = -\frac{1}{\rho_0} = -\frac{\frac{d^2\delta}{dx^2}}{\left[1 + \left(\frac{d\delta}{dx}\right)^2\right]^{3/2}}$$

If deflection is small, the slope term in the denominator vanishes, and the curvature is approximately equal to the second derivative of deflection.

$$\frac{M(x)}{EI} = -\frac{d^2\delta}{dx^2}$$

$$\theta(x) = \frac{d\delta}{dx}$$

Integrating the system of differential equations produces the following indefinite solutions.

$$V(x) = C_1 - \int_0^x w(s)ds$$

$$M(x) = C_2 + C_1 x - \int_0^x w(s)(x-s)ds$$

$$\theta(x) = C_3 - \frac{C_2 x}{EI} - \frac{C_1 x^2}{2EI} + \frac{1}{2EI}\int_0^x w(s)(x-s)^2 ds$$

$$\delta(x) = C_4 + C_3 x - \frac{C_2 x^2}{2EI} - \frac{C_1 x^3}{6EI} + \frac{1}{6EI}\int_0^x w(s)(x-s)^3 ds$$

Under the method of initial parameters, the constants of integration become the deflection, slope, moment, and shear where $x = 0$.

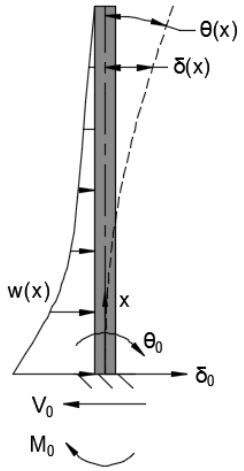

$$V(x) = V_0 - \int_0^x w(s)ds$$

$$M(x) = M_0 + V_0 x - \int_0^x w(s)(x-s)ds$$

$$\theta(x) = \theta_0 - \frac{M_0 x}{EI} - \frac{V_0 x^2}{2EI} + \frac{1}{2EI}\int_0^x w(s)(x-s)^2 ds$$

$$\delta(x) = \delta_0 + \theta_0 x - \frac{M_0 x^2}{2EI} - \frac{V_0 x^3}{6EI} + \frac{1}{6EI}\int_0^x w(s)(x-s)^3 ds$$

If the expected distributed load fits a third-order polynomial, the expressions become:

$$w(x) = a_0 + a_1 x + a_2 x^2 + a_3 x^3$$

$$V(x) = V_0 - a_0 x - \frac{a_1 x^2}{2} - \frac{a_2 x^3}{3} - \frac{a_3 x^4}{4}$$

$$M(x) = M_0 + V_0 x - \frac{a_0 x^2}{2} - \frac{a_1 x^3}{6} - \frac{a_2 x^4}{12} - \frac{a_3 x^5}{20}$$

$$\theta(x) = \theta_0 - \frac{M_0 x}{EI} - \frac{V_0 x^2}{2EI} + \frac{a_0 x^3}{6EI} + \frac{a_1 x^4}{24EI} + \frac{a_2 x^5}{60EI} + \frac{a_3 x^6}{120EI}$$

$$\delta(x) = \delta_0 + \theta_0 x - \frac{M_0 x^2}{2EI} - \frac{V_0 x^3}{6EI} + \frac{a_0 x^4}{24EI} + \frac{a_1 x^5}{120EI} + \frac{a_2 x^6}{360EI} + \frac{a_3 x^7}{840EI}$$

Bending strain is related to the moment expression in order to analyze the acquired strain gage data.

$$\varepsilon(x) = \frac{M_0 y}{EI} + \frac{V_0 y x}{EI} - \frac{a_0 y x^2}{2EI} - \frac{a_1 y x^3}{6EI} - \frac{a_2 y x^4}{12EI} - \frac{a_3 y x^5}{20EI}$$

The strain gages are located at a distance of $d/2$ from the neutral axis of the HP section. Substituting this into the bending strain expression:

$$\varepsilon(x) = \frac{M_0 d}{2EI} + \frac{V_0 d x}{2EI} - \frac{a_0 d x^2}{4EI} - \frac{a_1 d x^3}{12EI} - \frac{a_2 d x^4}{24EI} - \frac{a_3 d x^5}{40EI}$$

This expression can be simplified into the following fifth-order polynomial.

$$\varepsilon(x) = c_0 + c_1 x + c_2 x^2 + c_3 x^3 + c_4 x^4 + c_5 x^5$$

Where:

$$c_0 = \frac{M_0 d}{2EI} \qquad c_1 = \frac{V_0 d}{2EI} \qquad c_2 = -\frac{a_0 d}{4EI}$$

$$c_3 = -\frac{a_1 d}{12EI} \qquad c_4 = -\frac{a_2 d}{24EI} \qquad c_5 = -\frac{a_3 d}{40EI}$$

In order to solve for the coefficients based on acquired strain gage data, a least squares regression is implemented. This method produces a polynomial of a specified order k for n input strain gages.

$$\left\{\sum_{i=0}^{n-1} \varepsilon_i x_i^k\right\} = \left[\sum_{i=0}^{n-1} x_i^{k+l}\right]\{c_k\}$$

Or in expanded form for a fifth order regression:

$$\begin{Bmatrix} \sum_{i=0}^{n-1} \varepsilon_i x_i^0 \\ \sum_{i=0}^{n-1} \varepsilon_i x_i^1 \\ \sum_{i=0}^{n-1} \varepsilon_i x_i^2 \\ \sum_{i=0}^{n-1} \varepsilon_i x_i^3 \\ \sum_{i=0}^{n-1} \varepsilon_i x_i^4 \\ \sum_{i=0}^{n-1} \varepsilon_i x_i^5 \end{Bmatrix} = \begin{bmatrix} \sum_{i=0}^{n-1} x_i^0 & \sum_{i=0}^{n-1} x_i^1 & \sum_{i=0}^{n-1} x_i^2 & \sum_{i=0}^{n-1} x_i^3 & \sum_{i=0}^{n-1} x_i^4 & \sum_{i=0}^{n-1} x_i^5 \\ \sum_{i=0}^{n-1} x_i^1 & \sum_{i=0}^{n-1} x_i^2 & \sum_{i=0}^{n-1} x_i^3 & \sum_{i=0}^{n-1} x_i^4 & \sum_{i=0}^{n-1} x_i^5 & \sum_{i=0}^{n-1} x_i^6 \\ \sum_{i=0}^{n-1} x_i^2 & \sum_{i=0}^{n-1} x_i^3 & \sum_{i=0}^{n-1} x_i^4 & \sum_{i=0}^{n-1} x_i^5 & \sum_{i=0}^{n-1} x_i^6 & \sum_{i=0}^{n-1} x_i^7 \\ \sum_{i=0}^{n-1} x_i^3 & \sum_{i=0}^{n-1} x_i^4 & \sum_{i=0}^{n-1} x_i^5 & \sum_{i=0}^{n-1} x_i^6 & \sum_{i=0}^{n-1} x_i^7 & \sum_{i=0}^{n-1} x_i^8 \\ \sum_{i=0}^{n-1} x_i^4 & \sum_{i=0}^{n-1} x_i^5 & \sum_{i=0}^{n-1} x_i^6 & \sum_{i=0}^{n-1} x_i^7 & \sum_{i=0}^{n-1} x_i^8 & \sum_{i=0}^{n-1} x_i^9 \\ \sum_{i=0}^{n-1} x_i^5 & \sum_{i=0}^{n-1} x_i^6 & \sum_{i=0}^{n-1} x_i^7 & \sum_{i=0}^{n-1} x_i^8 & \sum_{i=0}^{n-1} x_i^9 & \sum_{i=0}^{n-1} x_i^{10} \end{bmatrix} \begin{Bmatrix} c_0 \\ c_1 \\ c_2 \\ c_3 \\ c_4 \\ c_5 \end{Bmatrix}$$

After solving this system of equations, the initial parameters and load polynomial coefficients are calculated from the obtained regression coefficients.

$$M_0 = \frac{2EIc_0}{d} \qquad V_0 = \frac{2EIc_1}{d} \qquad a_0 = -\frac{4EIc_2}{d}$$

$$a_1 = -\frac{12EIc_3}{d} \qquad a_2 = -\frac{24EIc_4}{d} \qquad a_3 = -\frac{40EIc_5}{d}$$

APPENDIX B

WHEATSTONE BRIDGE DERIVATION

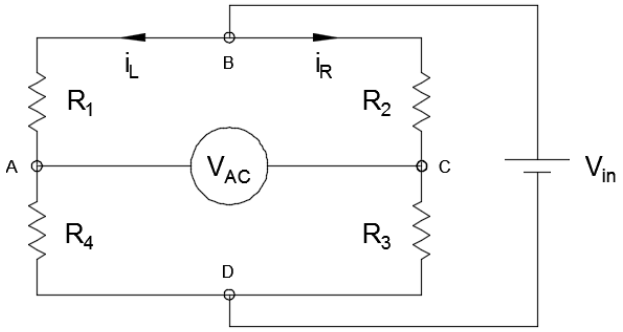

The relationship between voltage, current, and resistance is established with Ohm's Law:

$$V = iR$$

Assuming an initially balanced condition:

$$V_{AC} = 0$$

$$V_{BD} = i_R(R_2 + R_3) = i_L(R_1 + R_4) = V_{in}$$

$$i_R = \frac{V_{in}}{R_2 + R_3}\,, \qquad i_L = \frac{V_{in}}{R_1 + R_4}$$

Examining an unbalanced condition:

$$V_{AC} = V_{AD} - V_{CD} = i_L R_4 - i_R R_3$$

$$V_{AC} = \frac{V_{in}R_4}{R_1 + R_4} - \frac{V_{in}R_3}{R_2 + R_3} = V_{in}\left(\frac{R_4}{R_1 + R_4} - \frac{R_3}{R_2 + R_3}\right)$$

Defining resistance as a change from the initial condition:

$$R_1 = R_{1,0} + \Delta R_1\,, \qquad R_2 = R_{2,0} + \Delta R_2$$

$$R_3 = R_{3,0} + \Delta R_3\,, \qquad R_4 = R_{4,0} + \Delta R_4$$

$$V_{AC} = V_{in}\left(\frac{R_{4,0} + \Delta R_4}{R_{1,0} + \Delta R_1 + R_{4,0} + \Delta R_4} - \frac{R_{3,0} + \Delta R_3}{R_{2,0} + \Delta R_2 + R_{3,0} + \Delta R_3}\right)$$

If all resistors have the same initial resistance R:

$$V_{AC} = V_{in}\left(\frac{R + \Delta R_4}{2R + \Delta R_1 + \Delta R_4} - \frac{R + \Delta R_3}{2R + \Delta R_2 + \Delta R_3}\right)$$

The gage factor is a ratio of the fractional change in resistance to the axial strain of the gage. This quantity is specified by the manufacturer.

$$F_G = \frac{\Delta R/R}{\Delta L/L} = \frac{\Delta R/R}{\varepsilon}$$

$$\Delta R = \varepsilon R F_G$$

Substituting this expression into the equations for V_{AC}:

$$V_{AC} = V_{in}\left(\frac{R + \varepsilon_4 R F_G}{2R + \varepsilon_1 R F_G + \varepsilon_4 R F_G} - \frac{R + \varepsilon_3 R F_G}{2R + \varepsilon_2 R F_G + \varepsilon_3 R F_G}\right)$$

$$V_{AC} = V_{in}\left(\frac{1 + \varepsilon_4 F_G}{2 + \varepsilon_1 F_G + \varepsilon_4 F_G} - \frac{1 + \varepsilon_3 F_G}{2 + \varepsilon_2 F_G + \varepsilon_3 F_G}\right)$$

If any of the gages in the bridge are substituted with fixed resistors, the values of ε become 0 as no change in resistance occurs. In the case of the strain gage setup for this project, resistors 3 and 4 are fixed, and the associated strains are $\varepsilon_3 = \varepsilon_4 = 0$.

$$V_{AC} = V_{in}\left(\frac{1}{2 + \varepsilon_1 F_G} - \frac{1}{2 + \varepsilon_2 F_G}\right)$$

In addition to measuring strain, the experimental setup provides compensation for thermal expansion and contraction. In all of the bridges, resistor 2 is a thermal

dummy gage. If total strain along the axis of a gage is a combination of mechanical and thermal strain, then ε_2 must be subtracted from each strain value.

$$V_{AC} = V_{in}\left(\frac{1}{2 + (\varepsilon_1 - \varepsilon_2)F_G} - \frac{1}{2}\right)$$

Input and output voltages are directly measured, and the gage factor is specified by the manufacturer. The quantity required for further analysis can be obtained by rearranging the equation and substituting in the temperature compensated strain.

$$\varepsilon = \varepsilon_1 - \varepsilon_2$$

$$\varepsilon = \frac{1}{F_G}\left[\frac{1}{\frac{V_{AC}}{V_{in}} + \frac{1}{2}} - 2\right]$$

Strain measurements for gages oriented in the transverse direction must be converted to longitudinal strain using Poisson's ratio, ν.

$$\varepsilon_L = -\frac{\varepsilon_T}{\nu}$$

APPENDIX C

INSTRUMENTATION WIRING DIAGRAMS

Illustration credits: Rachal, 2014

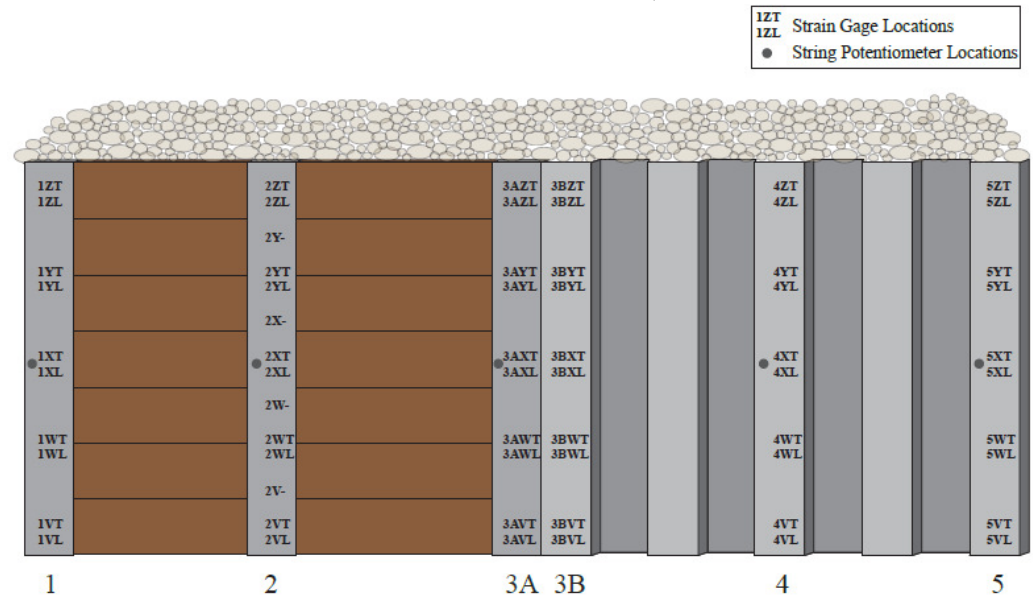

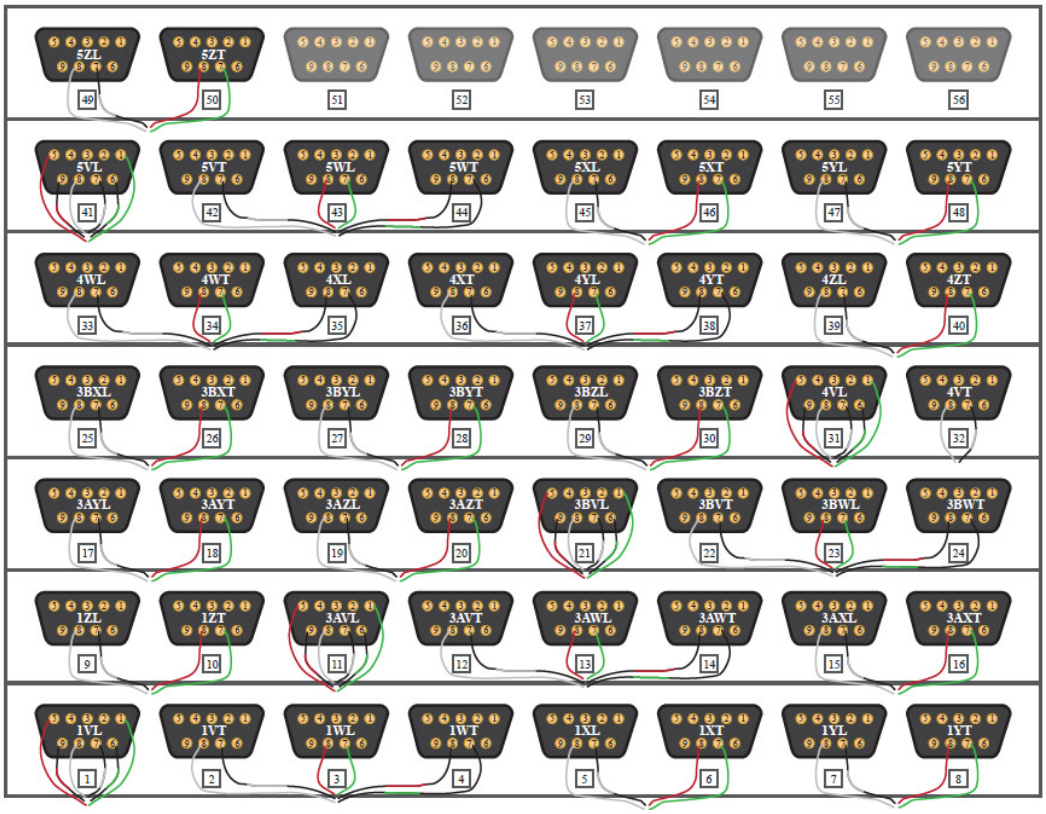

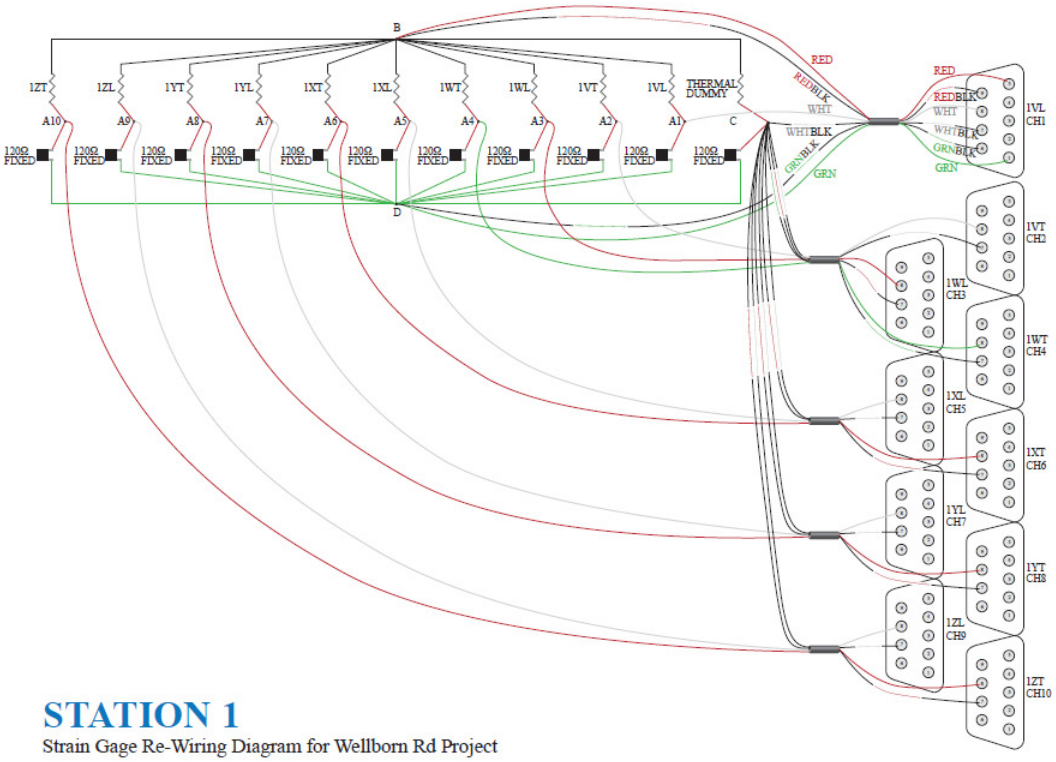

STATION 1

Strain Gage Re-Wiring Diagram for Wellborn Rd Project

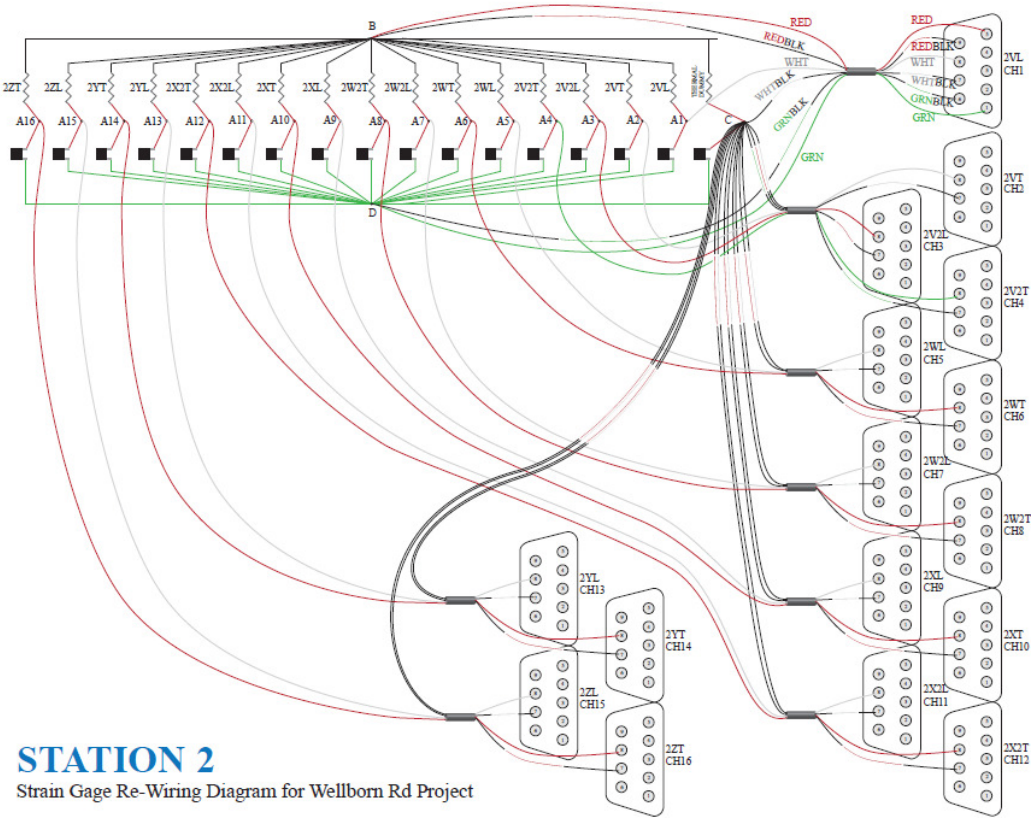

STATION 2

Strain Gage Re-Wiring Diagram for Wellborn Rd Project

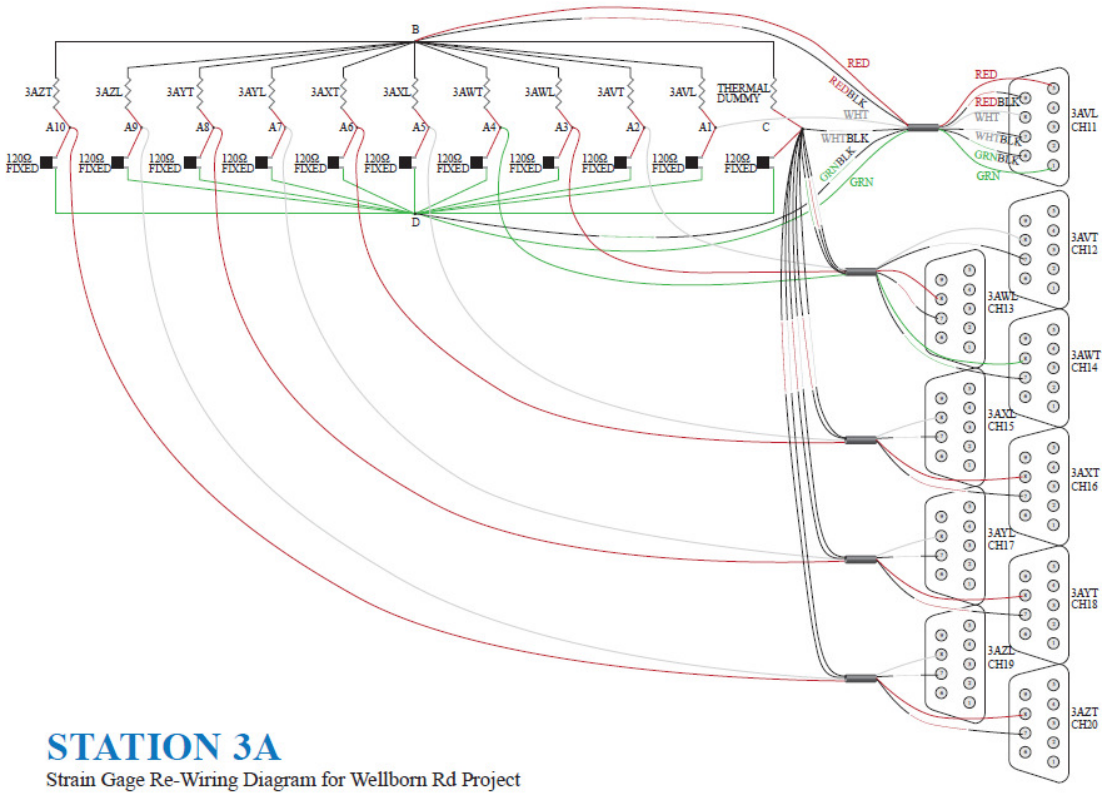

STATION 3A

Strain Gage Re-Wiring Diagram for Wellborn Rd Project

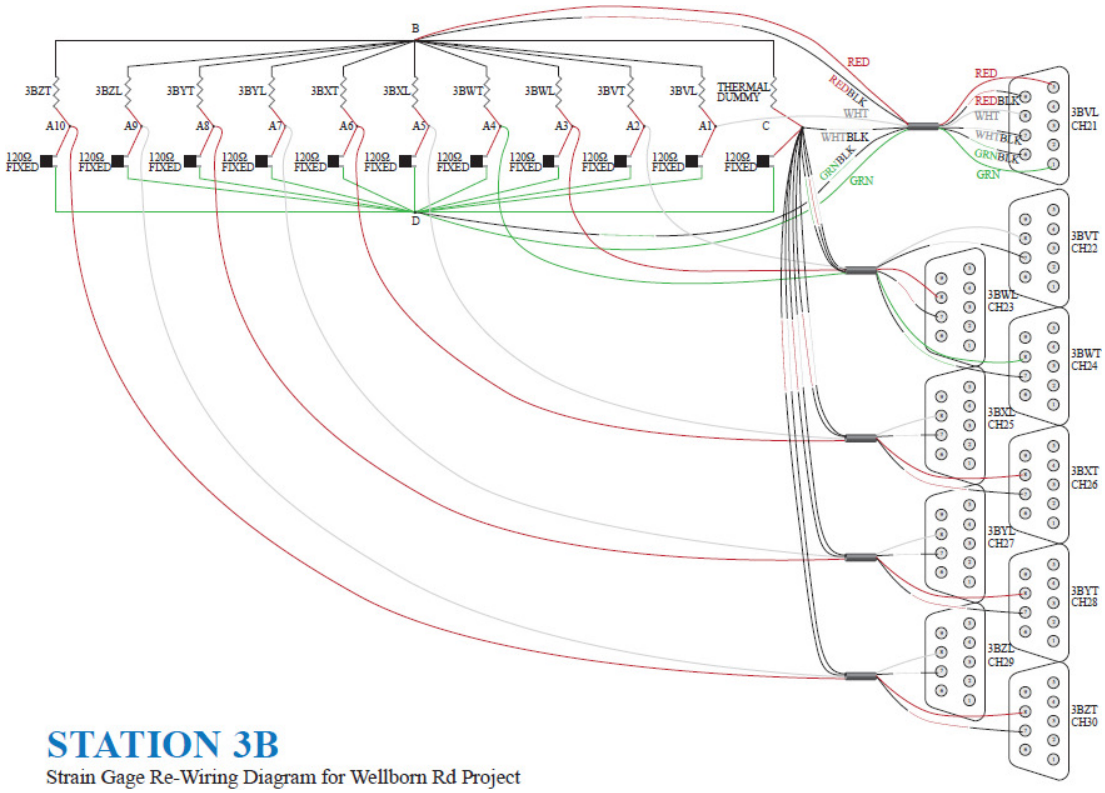

STATION 3B

Strain Gage Re-Wiring Diagram for Wellborn Rd Project

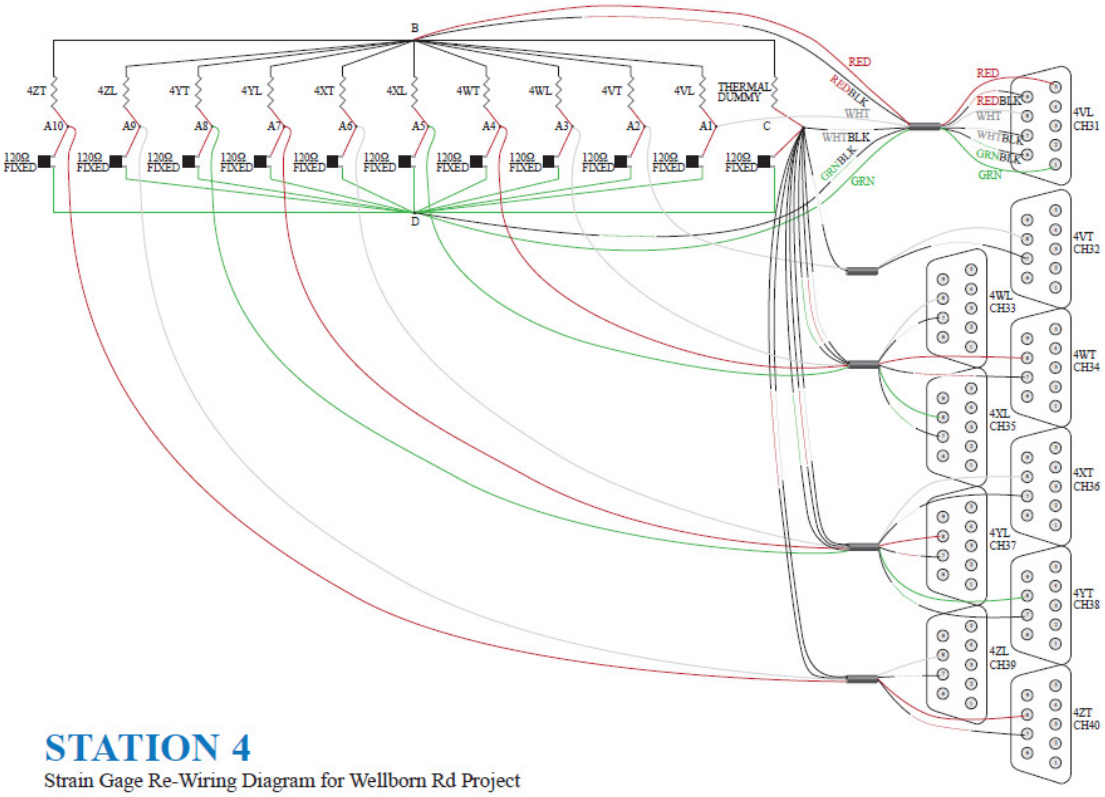

STATION 4

Strain Gage Re-Wiring Diagram for Wellborn Rd Project

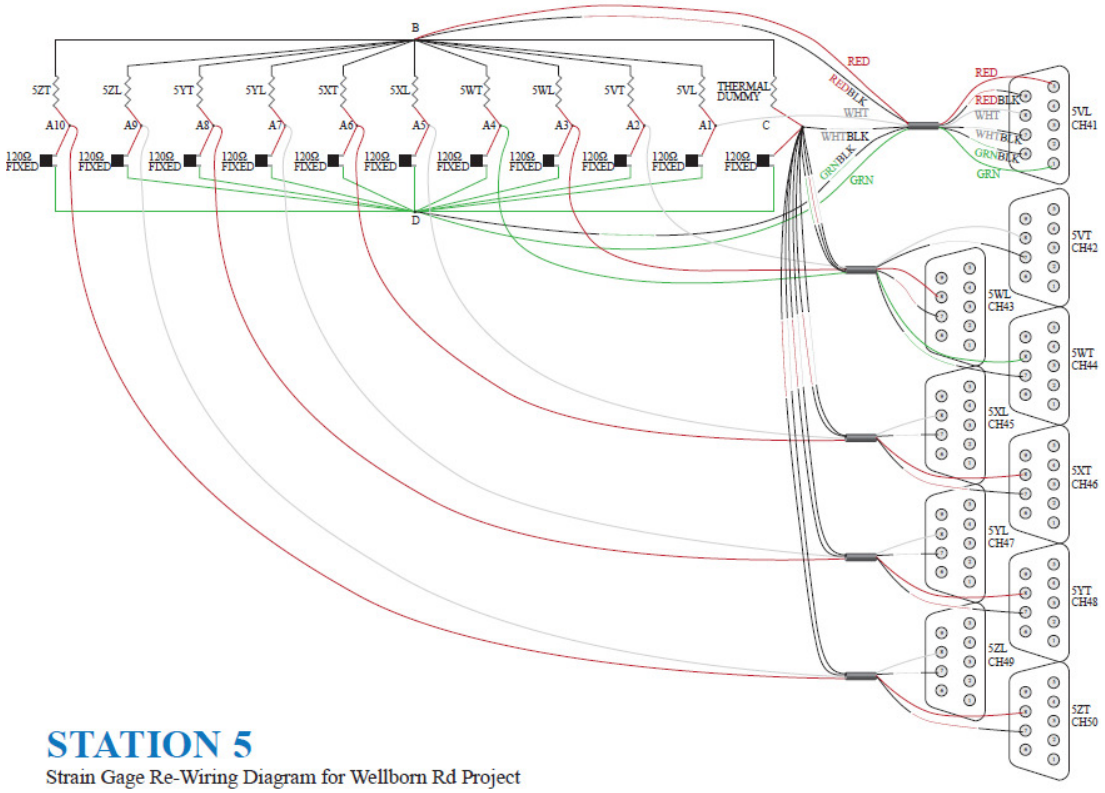

STATION 5

Strain Gage Re-Wiring Diagram for Wellborn Rd Project

APPENDIX D

CODE LISTING OF WALL_STRESS.PY

```
# ======================================================================
# Retaining Wall Analysis Module
# Sean Smith
# v1.2 - 10 Jun 2016
# ======================================================================
# Version History
# 1.0 - 20 Jan 2016
# - Initial release of program
#
# 1.1 - 26 Feb 2016
# - Upgraded to Python 3.5
# - Modified analysis to perform Least Squares regression
#
# 1.2 - 10 Jun 2016
# - Version implemented in thesis appendix
# ======================================================================
# Built using Python 3.5 and the following external libraries:
# - numpy: http://www.numpy.org/
# - openpyxl: https://openpyxl.readthedocs.org/
# Note: Some arrays use 64-bit precision
# ======================================================================
# This program is used for analyzing strain gage data on a retaining
wall.
# Another program was written in MATLAB to perform the same function,
# but this one finishes 500 times faster.
#
# To use this program, skip the next few lines and go to the user-
defined
# parameters section. Enter details specific to the retaining wall,
# specify the input/output filename, and run the program. Output file
# will be created in the same project folder as this program.
# ======================================================================
# Input Excel file columns:
# A - Time (s)
# B:end - Strain values (unitless)
#
# Output Excel file columns:
# A - Time (s)
# B - Moment at x=0 (kip-in.)
# C - Shear at x=0 (kips)
# D:D+n - distributed load coefficients (n = polynomial order)
# D+n+1:end - stress at each strain gage (ksi) (e_count = # of gages)
# ======================================================================
```

```
# Imports necessary libraries
import numpy as np                  # numpy offers better handling of
arrays
import time                         # time calculates total computation
time
import math as m                    # math is used specifically for
factorials in this program
import os                           # os manipulates files in the file
system
from openpyxl import load_workbook  # openpyxl.load_workbook loads
Excel data for analysis
from openpyxl import Workbook       # openpyxl.Workbook creates and
saves output workbook

start_time = time.time()

# DO NOT CHANGE ANYTHING ABOVE THIS POINT
# ======================================

# Specifies user-defined parameters
# HP12X84 section. Refer to AISC Shapes Database for section properties
E = 30000                           # Elastic modulus (ksi)
I = 650                             # Moment of inertia (in.^4)
d = 12.3                            # Cross-section depth (in.)

x = np.array([0.,1.,2.,3.,4.,5.,6.,7.])  # Location of strain gages on
wall (ft)
e_count = 8                         # Number of strain gages
n = 3                               # Order of polynomial of
distributed load

file_no_extension = 'UP_Wall'       # Name of the input Excel file
without the .xlsx part

# DO NOT CHANGE ANYTHING BELOW THIS POINT
# ======================================

# Converts user defined values for simpler calculation
EI = E*I
x = np.transpose(x)
x=x*12

# Raises exception if order of the linear system exceeds number of
available strain gages
if n+3 > e_count:
    raise Exception('Order of solution exceeds number of strain gages.
Reduce value of n.')

# Defines input and output files
file_in = file_no_extension+'.xlsx'
file_out = file_no_extension+'_analyzed.xlsx'

# Reads input Excel file (openpyxl library)
```

```
wb_in = load_workbook(filename = file_in, data_only=True)
sheets_in = wb_in.worksheets
tests = len(sheets_in)

# Creates output Excel file
if os.path.isfile(file_out):
    os.remove(file_out)
wb = Workbook()
wb.save(file_out)
wb_out = load_workbook(filename = file_out)

x_space = np.linspace(0,x[-1],(x[1]-x[0])*10+1)

# Loops through each sheet in the input workbook
for i in range(0, tests):
    loop_time = time.time()

    # Prepares output and input files for current test
    ws = wb.create_sheet()
    ws.title = str(i+1)
    curr_sheet_in = sheets_in[i]
    full_data=np.array(curr_sheet_in.columns)

    # Puts input data into separate arrays
    t_full = np.array(full_data[0])
    t = t_full[1:]
    t = t[:,np.newaxis]
    e_full = np.transpose(np.array(full_data[1:]))
    e = e_full[1:]

    # Preallocates output arrays
    M0 = np.zeros([len(t),1])
    V0 = np.zeros([len(t),1])
    a = np.zeros([len(t),n+1])
    sigma = np.zeros([len(t),e_count])
    final_array = np.zeros([len(t),n+e_count+4])

    # Define sheet header array
    head_array = np.empty((1,4+n+e_count), dtype=object)
    head_array[0,0] = 't (s)'
    head_array[0,1] = 'M0 (k-in)'
    head_array[0,2] = 'V0 (kips)'
    for j in range(0,n+1):
        head_array[0,j+3] = 'a'+str(j)
    for j in range(0,e_count):
        head_array[0,j+n+4] = 'sigma'+str(j)+' (ksi)'

    # Loops through each data point in the acquired data
    for j in range(0,len(t)):
        e_new = np.zeros([n+3,1])
        X = np.zeros([n+3,n+3])

        # Builds and solves linear system e_new=X*c
```

```
        for k in range(0,n+3):
            for l in range(0,n+3):
                for q in range(0,len(x)):
                    X[k,l] = X[k,l] + x[q]**(k+l)
            for l in range(0,len(x)):
                e_new[k,0] = e_new[k,0] + (-e[j,l].value)*x[l]**(k)
        c = np.linalg.solve(X,e_new)

        # Calculates initial parameters and load coefficients
        M0[j,0] = -2*EI*c[0,0]/d
        V0[j,0] = -2*EI*c[1,0]/d
        for k in range(0,n+1):
            a[j,k]=(2*EI*c[k+2,0]/d)*m.factorial(k+2)/m.factorial(k)
        for k in range(0,e_count):
            sigma[j,k]=E*(e[j,k].value)
        t[j,0]=t[j,0].value

        # Prepares output data for entry into Excel
        final_array[j,0] = t[j,0]
        final_array[j,1] = M0[j,0]
        final_array[j,2] = V0[j,0]
        for k in range(0,n+1):
            final_array[j,k+3] = a[j,k]
        for k in range(0,e_count):
            final_array[j,k+n+4] = sigma[j,k]

        y = np.zeros(len(x_space))
        for k in range(0,len(x_space)):
            for l in range(0,n):
                y[k] = y[k]+a[j,l]*x_space[k]**l

    # Writes header and output rows to Excel
    for j in range(0,head_array.shape[1]):
        ws.cell(row = 1, column = j+1).value = head_array[0,j]
    for j in range(0,final_array.shape[0]):
        for k in range(0,final_array.shape[1]):
            ws.cell(row = j+2, column = k+1).value = final_array[j,k]

    # Displays time to run current test
    loop_end_time = time.time()-loop_time
    print('Test '+str(i+1)+' time elapsed: '+str(loop_end_time)+'
seconds')

# Deletes default 'Sheet' sheet
bad_sheet = wb.get_sheet_by_name('Sheet')
wb.remove_sheet(bad_sheet)

# Displays final calculation time
wb.save(file_out)
end_time = time.time()-start_time
print('Final time elapsed: '+str(end_time)+' seconds')
print('Analysis complete. Check output file.')
```